CONTROLLING LIGHT INSIDE A MULTI-MODE FIBER BY WAVEFRONT SHAPING

A THESIS SUBMITTED TO
THE GRADUATE SCHOOL OF NATURAL AND APPLIED SCIENCES
OF
MIDDLE EAST TECHNICAL UNIVERSITY

BY
HALİL İBRAHİM BİNİCİ

IN PARTIAL FULFILLMENT OF THE REQUIREMENTS
FOR
THE DEGREE OF MASTER OF SCIENCE
IN
MICRO AND NANOTECHNOLOGY

JANUARY 2018

Approval of the thesis:

CONTROLLING LIGHT INSIDE A MULTI-MODE FIBER BY WAVEFRONT SHAPING

submitted by **HALİL İBRAHİM BİNİCİ** in partial fulfillment of the requirements for the degree of **Master of Science in Micro and Nanotechnology Department, Middle East Technical University** by,

Prof. Dr. Gülbin Dural Ünver _______________
Dean, Graduate School of **Natural and Applied Sciences**

Assoc. Prof. Dr. Burcu Akata Kurç _______________
Head of Department, **Micro and Nanotechnology**

Asst. Prof. Dr. Emre Yüce _______________
Supervisor, **Physics Dept., METU**

Asst. Prof. Dr. Serdar Kocaman _______________
Co-Supervisor, **Electrical and Electronical Eng. Dept., METU**

Examining Commitee Members:

Assoc. Prof. Dr. Halil Berberoğlu _______________
Physics Dept., Gazi University

Asst. Prof. Dr. Emre Yüce _______________
Physics Dept., METU

Asst. Prof. Dr. Selçuk Yerci _______________
Micro and Nanotechnology, METU

Assoc. Prof. Dr. Alpan Bek _______________
Physics Dept., METU

Assoc. Prof. Dr. Serhat Çakır _______________
Physics Dept., METU

Date: 30.01.2018

I hereby declare that all information in this document has been obtained and presented in accordance with academic rules and ethical conduct. I also declare that, as required by these rules and conduct, I have fully cited and referenced all material and results that are not original to this work.

Name, Last name : Halil İbrahim BİNİCİ

Signature :

ABSTRACT

CONTROLLING LIGHT INSIDE A MULTI-MODE FIBER BY WAVEFRONT SHAPING

Binici, Halil İbrahim

M.Sc, Micro and Nanotechnology

Supervisor: Asst. Prof. Dr. Emre Yüce

Co-Supervisor: Asst. Prof. Dr. Serdar Kocaman

January 2018, 70 pages

Light is the primary tool used for collecting information from macroscopic and microscopic structures of matter. Micro-nano technology based materials like microcavities, waveguides, photonic crystals and fibers are used for confining light in space and the latter enable long distance information transfer. To increase the capacity of an information link, the core size of an optical fiber must be increased. Due to increased size of the fiber, the number of supported modes increases and becomes a multi-mode fiber. Given the increased number of modes, interference starts to play a major role and a random speckle pattern forms at the output of the fiber. In this thesis speckle pattern is controlled via controlling interference of the fiber modes by controlling relative phase among the guided modes.

Wavefront shaping is developed for guiding light through highly scattering materials by spatially modulating the wavefront of an incident coherent beam. The most common way to shape the wavefront is to use a spatial light modulator (SLM). SLMs can be used to modulate the phase of a guided mode when employed at the input of an optical fiber as a spatial filter. As a result, the intensity pattern at the output plane can be controlled. In fact, the speckle pattern that is forming at the output of a multimode optical fiber can be concentrated to a single spot.

In this thesis, we provide methods to control output of an optical fiber for developing advanced technologies for life sciences and communication technologies.

Keywords: Multimode Fibers, Wavefront Shaping, Speckle Pattern, Interference

ÖZ

DALGA ÖNÜ ŞEKİLLENDİRMESİ İLE ÇOK MODLU FİBERDE IŞIK KONTROLÜ

Binici, Halil İbrahim

Yüksek Lisans, Mikro ve Nanoteknoloji

Tez Yöneticisi: Yard. Doç. Dr. Emre Yüce

Yardımcı Tez Yöneticisi: Yard. Doç. Dr. Serdar Kocaman

Ocak 2018, 70 sayfa

Işık, maddenin mikro ve makro ölçekteki yapılarından veri toplamak için kullanılan temel bir araçtır. Mikrokovuklar, dalga kılavuzları, fotonik kristaller ve fiber gibi mikro ve nano teknolojik bazlı malzemeler ışığın uzayda sınırlandırılması ve uzun mesafeli veri transferi için kullanılır. Veri bağlantısının kapasitesini arttırmak için fiber çekirdek büyüklüğü arttırılmalıdır. Arttırılan fiber büyüklüğü ile beraber ortamda desteklenen modların sayısı artmış olup fiber çok modlu bir fiber haline gelmiştir. Artan mod sayısıyla birlikte girişim büyük bir rol oynayıp, fiber çıkışında rastgele alacalı bir desen oluşur. Bu alacalı desen, fiber modlarının girişimini kontrol etmek aracılığıyla modlar arasındaki görece fazı değiştirerek kontrol edilir.

Dalga önü şekillendirmesi, fazla saçıcı ortamdan geçen koherent ışığın dalga önünün uzaysal şekillendiirlmesiyle geliştirilmiştir. Dalga önünü şekillendirmek için kullanılan en bilinen yöntem uzaysal ışık modülatörü (SLM) kullanmaktır. Fiber optiğin girişinde bir uzaysal filtre gibi kullanılan uzaysal ışık modülatörleriyle, desteklenen modların fazları kontrol edilebilir. Böylece, fiber sonundaki güç dağılımı kontrol edilebilir. Öyle ki çok modlu fiberin sonunda oluşturulan alacalı desen tek bir noktaya toplanılabilir.

Bu tezde yaşam ve iletişim bilimleri için gelişmiş teknolojiler geliştirmek için fiber optik sonunu kontrol etmeyi sağlayacak metodlar geliştirilecektir.

Anahtar Sözcükler: Çok Modlu Fiber, Dalga Önü Şekillendirmesi, Alacalı Desen, Girişim

To my father, İsmail

ACKNOWLEDGEMENTS:

Firstly, I would like to thank Asst. Prof. Dr. Emre Yüce for accepting as a student. Without his trust and guidance, I can hardly finish my work. His faith to me became the most encouraging factor to finish my thesis.

I would like to thank my colleagues Yalın, Mehmet, Şahin, Anıl, Nezir and Sait in Programmable Photonics Group for their friendship and support.

I would like to thank examing commitee members Halil Berberoğlu, Selçuk Yerci, Alpan Bek and Serhat Çakır and my co-advisor Serdar Kocaman for their ideas to improve my thesis.

I would like to thank Nergis Ayan for her love and faith to me. When I felt desperate, she motivated to focus on my work.

Finally, I would like to thank my family, İsmail, Emel, Elif and Abdülsamet for their understanding, moral and financial support during my master study.

TABLE OF CONTENTS

LIST OF FIGURES

FIGURES

LIST OF TABLES

TABLES

NOMENCLATURE

E	Electric Field
H	Magnetic Field
LP	Linearly Polarized
NA	Numerical Aperture
r_{corr}	Correlation Constant
TE	Transverse Electric
TM	Transverse Magnetic
SLM	Spatial Light Modulator
V-Number	Normalized Frequency
α_n	Cross-correlation between Fields
β	Propagation Constant
ε_0	Electrical Permittivity of Free Space
μ_0	Magnetic Suspectibility of Free Space
κ	Transverse Parameter of Fiber in the Core
σ	Transverse Parameter of Fiber in the Cladding
ψ	Wave Field

CHAPTER I

INTRODUCTION

Optical fibers enables to confine and transfer light for long distances. They are used for telecommunication, imaging, spectroscopy and medical treatment. The total intensity distribution at the output of the multimode fiber is determined by interference of the supported modes which are defined as the propagation planes of the light rays in the waveguide. In our thesis, the intensity distribution at the output is controlled by changing phase of the modes.

By controlling these modes, the total intensity at the output whether increased or decreased. Increasing total intensity at the output of the fiber enables to new opportunities in biophotonics. It makes deep imaging through tissue possible. Moreover, the light can be optimized to a single spot in the fiber by addition phases to modes.

1.1. Propagation of Light in Complex Media:

When light interacts with matter, it can be absorbed, transmitted or scattered. Light propagating through materials having inhomogeneties, such as egg shell, paper, white paint or biological tissue is mostly scattered. Only small portion of light is transmitted. Scattering of the light makes imaging the medium impossible in deep portions. The theoretical explanation of scattering is explained by mesoscopic physics[1-10], quantum transport of electrons and photons[11-13] and random matrix theory[14-15].

In order to eliminate the effect of the scattering, the spatial phase of light can be controlled via interaction in a designed medium. Liquid crystals provide the means to gain control on light propagation in a programmable manner.

1.2. Wavefront Shaping:

Wavefront shaping is a powerful method developed for going control on propagation of light in complex media. It has been used for more than a decade to control the light inside turbid medium[16]. Inside the turbid medium, light scattered from microsized impurites. In 60s, the wavefront distortions of light due to atmosphere can be corrected by controlling a dozen of optical elements to make astronomical observations[17]. After invention of micro-mirror or liquid crystal based spatial light modulators (SLM), millions of pixels on the same chip is controlled given opportunities to program spatial phase of light. This invention provides million degrees of freedom to control light spatially.

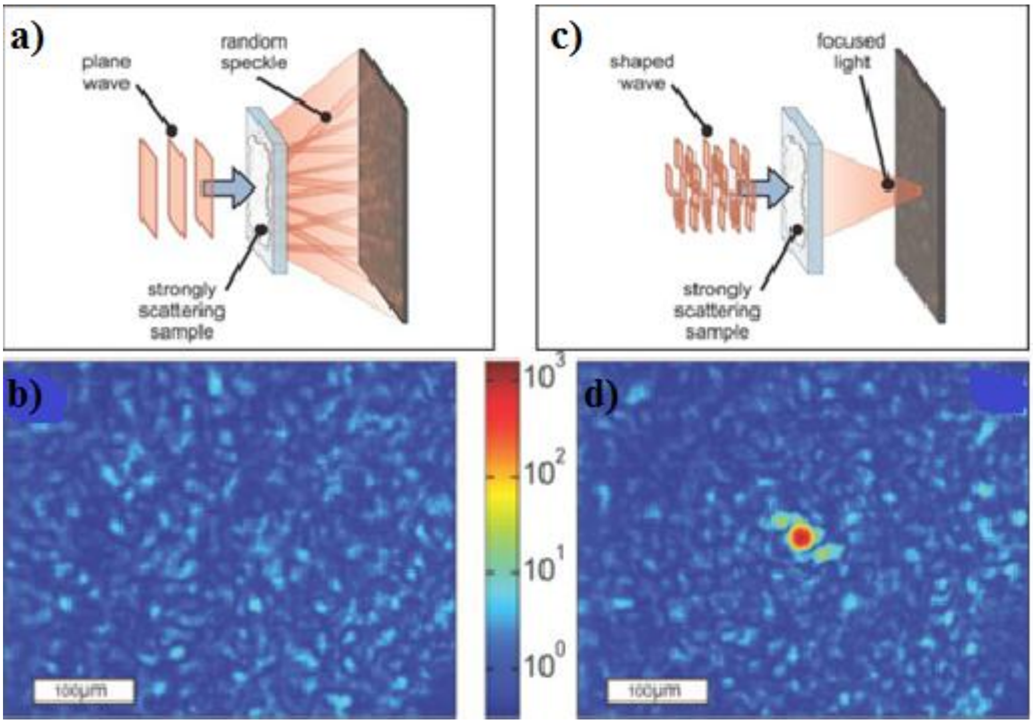

Figure 1.1. a) Plane waves passing through turbid medium and forming speckle b) Intensity distribution before the optimization c) Shaped wave passing through turbid medium and focused to a single spot. b) Intensity distribution after the optimization. The figure is adapted from [18].

In 2007[18], Vellekoop and Mosk made a poineer experiment to manipulate and focus light through opaque and scattering materials by controling the wavefront of the incident beams. In this paper, Vellekoop and Mosk used a liquid crystal based spatial light modulator (SLM) to control phases each segment of incoming beam through scattering medium. Therefore, when the modulated beams passed through scattering medium, the optimized bright spot is formed at the output. This experiment showed by controlling phases of incoming light, the optimized spot could be obtained. Vellekoop et al used the scattering media as opaque lens by manipulation of light.[19]

As well as optimized spots, complex fields[20-21] could be created. From the work of Vellekoop and Mosk to today, wavefront shaping has been using to investigate physical optics phenomena like determination of open transmission eigenchannels[22] spectral control[23], polarization modulation[24-25], spatiotemporal modulation[26], optical phase conjugation[27], improvement of Raman scattering in turbid medium[28], Kerr nonlinearity managament[27-29], near-field control[29], optimization of Wigner-Smith operator[30] and engineering Bessel modes[31]. The method has employed many applications like two-photon microscopy[32], imaging through biological tissues[33-34], optical coherence tomography[35], optogenetics[36], solar cell[37], scattering optical elements[38], 3D holographic displays[39], laser processing[40] compressive imaging[41] and generation of quantum-secure classical keys[42].

1.3. Multimode Fiber Optics as Scattering Medium:

Modes are the propagation planes of waves along optical fibers. The optical fibers are catagorised in terms of their number of modes: single-mode and multi-mode operation. In single-mode fibers, there is ony way to enter the waveguide within its numerical aperture and the waveguide supports only one mode to propagate. Therefore, there is one propagation channel in the waveguide which makes it prefferable for long distance communication. The core diameter of single mode fibers is around 8 μm[43] at telecom wavelength.

In multimode fibers, when coherent light source enters optical fiber, the light splits into supported modes with different propagation constants. Therefore, it can be said that multimode fiber could behave as scattering medium. The number of the present modes gives the large number of degrees of freedom. This allows to increase information capacity of optical fibers as compared to single mode fibers. The larger mode core are of multimode fibers and the propagation of energy through spatial modes weaken the nonlinear effects which makes multimode fibers prefferable for high power applications.

By using SLM, multimode fibers can be used for enhanced imaging[44-51], broadband fiber spectrometer[52] , 3D micro-fabrication[53] and demultiplexing of mode groups[54], observing principal[55-56], super-principal and anti-principal modes[57],measurement of transmission matrix[58-59] and flourescence[60] photoacoustic[61] microscopies.

1.4. The Effect of Wavelength on Speckle Pattern:

In a multimode fiber, interference of guided modes creates a wavelength dependent speckle pattern at the output of the fiber. From wavelength dependent speckle pattern, temperature[62], pressure[63] or acoustic vibrations[64-65] can be sensed.

In studies of Cao et al[66-67], multimode fiber was used as high resolution low loss spectrometer. Transmission matrix based algorithm was developed to recover the speckle pattern in the presence of noise. They achieved 0.15 nm spectral resolution over 25 nm bandwith using 1 m fiber and 0.03 nm spectral resolution over 3 nm bandwith using 5 m fiber. All-fiber based spectrometers have advantages like high spectral resolution, lower cost compared to traditional spectrometers due to all-fiber structures and low insertion loss.

In Fig.1.2., the speckle change with changing wavelength of the light is shown both graphically (a)) and analytically (d)). From Fig.1.3.(b). as wavelength of coherent source changes, correlation between speckles with changing wavelength drops faster and the spectral correlation length decreases. One of our objective in thesis is investigation of optimization of intensity on the correlations between speckles.

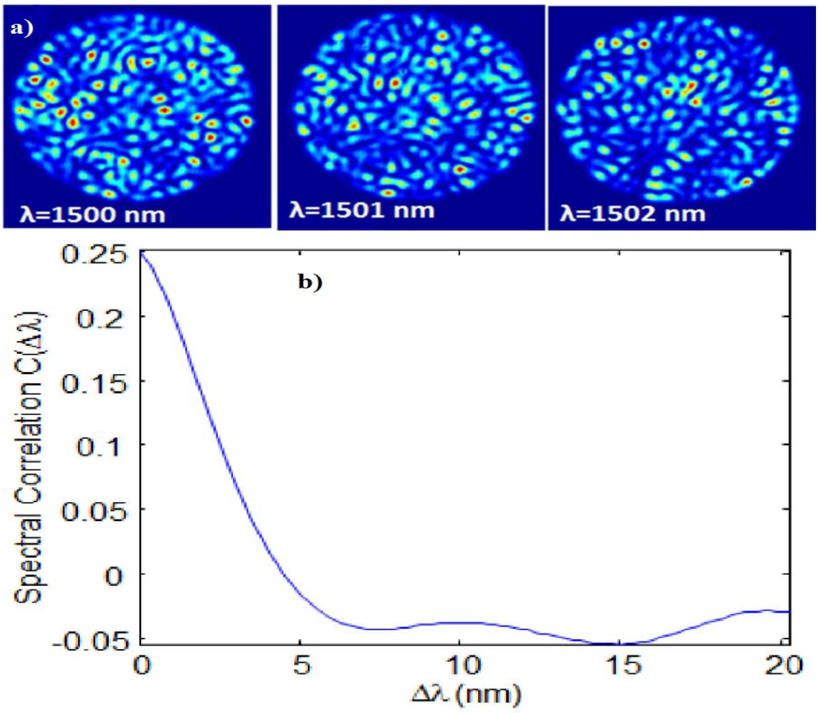

Figure 1.2. a) Images of intensity distribution of speckle patterns at the output of the 5 m long fiber. b) Spectral correlation function C(Δλ) normalized to unity at Δλ = 0 for changing wavelength within Δλ = 20 nm. The figure is adapted from [66-67].

In this thesis, we will intestigate the effect of wavelength on speckle patterns in both unoptimized and optimized cases by observing correlation between speckles.

1.5. Spatial Mode Division and Multiplexing:

In single mode fibers, the light can propagate only one channel. In order to increase the capacities of fibers, each supported mode in the waveguide can be used as transmission channel. As it is shown from Fig.1.4., information can be modulated through the supported modes with the appropriate optical design. With this technique, high data transfer rates can be achieved for silicon photonics[68] and optical fibers[69].

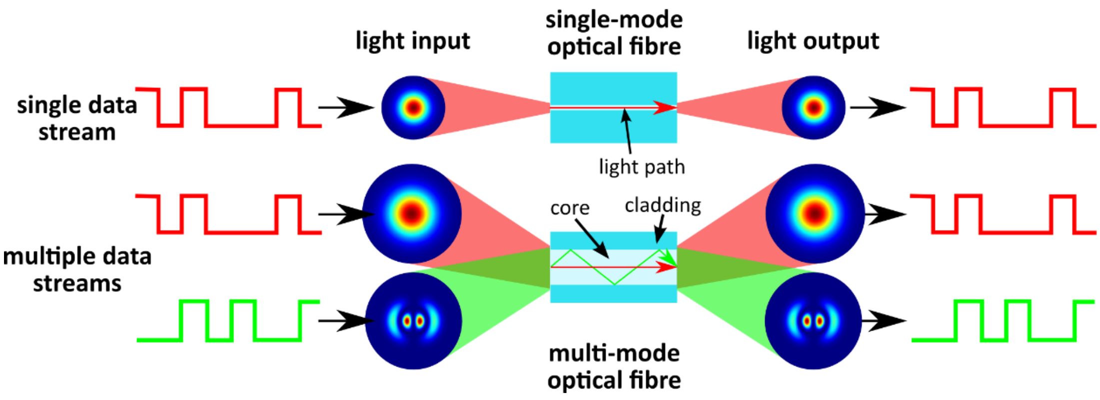

Figure 1.3. The principle of Mode Division Multiplexing. The figure is adapted from [70].

In work of Carpenter et al[55], they introduced modulating and demultiplexing of modes in an optical fiber by using SLM. In Fig.1.5., creation of multichannel system is shown by multiplexing of two modes and focusing different channels is shown by phase mask writing as filtering element on SLM surface. By demultiplexing of modes, the phases of modes can be controlled individually. In our study, we control few modes individually in order to observe local intensity changes in the fiber.

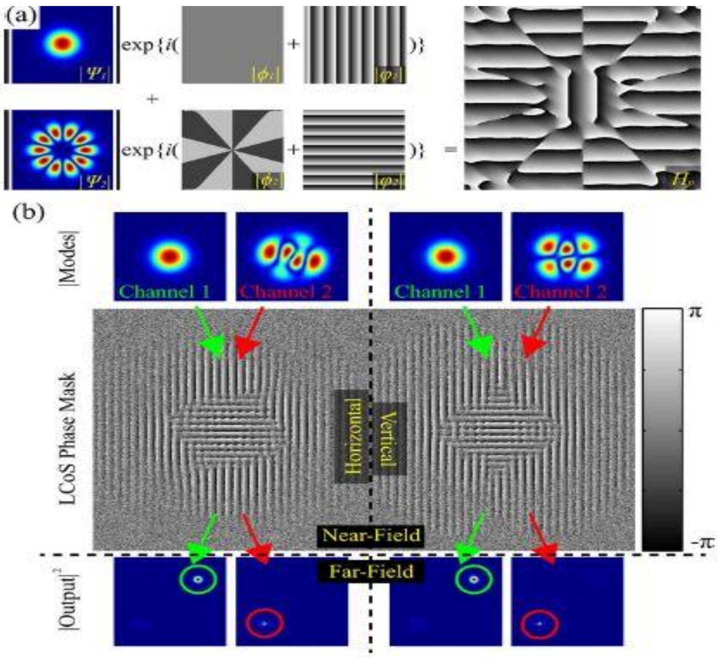

Figure 1.4. a) Construction of multichannel system with two modes b) The phase mask written on SLM surface demultiplexing of the multichanel system. The figure is adapted from [55].

In this thesis, we study theoretical investigation of manipulation of present modes of multimode fibers. By manipulating these modes, we investigate increasing, decreasing intensities of core of the fibers and forming an optimized spot. We show by manipulating a mode and a group of mode inside the fiber, the intensity increases by nearly 2 times within a small area inside the core of optical fiber. Also, the effect of frequency of light on speckle also is investigated.

1.6. Overview of the Thesis:

In Chapter II, we discuss theory of propagation of light inside multimode fiber. The scalar wave equation of cylindrical waveguides solved. By solving this equation we get three different polarizations: TE, TM and hybrid modes. However, using weakly guiding approximation, we use linearly polarized modes to solve field equations inside the waveguides.

In Chapter III, the results of calculations are shown and analyzed. There are two main calculatons: intensity calculations and frequency correlation. In first one, speckle pattern of optical fibers without any phase addition are calculated. After that random phases are added to modes to observe any perturbation like bending or inhomogenities of refractive index distribution of the optical fiber. The effect of wavelength of coherent source on speckle pattern is also examined within $\Delta\lambda = 4$ nm. After these intensity calculations, we made optimizations of speckle patterns at the output of a multimode fiber by increasing, decreasing intensities and creating a spot. Finally, the intensity change is inspected by changing phase of one and two modes.

In Chapter IV, assumptions while performing calculations and results in the thesis are discussed.

CHAPTER II

WAVE THEORY OF OPTICAL WAVEGUIDES

2.1.Ray Optics of Propagation of Light:

An optical waveguide is composed of a core where light is confined and a cladding which surrounds the core as shown Fig.2.1. For confinement of light inside waveguide, the refractive index of the core n_1 must be higher than that of cladding n_0. Light propagates inside such a waveguide by hitting core-cladding interface and reflecting from there. At certain angles light can bt totally reflected from this interface.

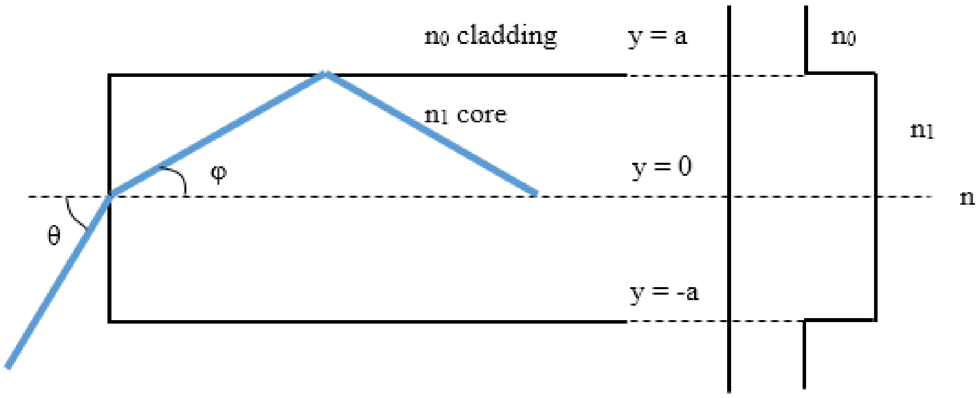

Figure 2.1. The structure of optical fiber and ray picture of propagation of light inside optical fiber

The condition for the total internal reflection is given by $n_1*\sin(\pi/2-\varphi) \geq n_0$. The entrance angle φ is related to incoming angle θ and the relation is given by $\sin\theta = n_1*\sin\varphi \leq (n_1^2-n_0^2)^{0.5}$ using which the following relation can be obtained:

$$\theta \leq \sin^{-1}\sqrt{n_1^2 - n_0^2} = \theta_{max} \qquad \text{Eq.2.1.}$$

Eq.2.1 gives θ_{max} the maximum acceptance angle θ_{max} of an optical fiber which defines the numerical aperture (NA) of a waveguide NA can be expressed by using the relative refractive index (Δ) and core refractive index (n_1) as follows:

$$\theta_{max} = NA = n_1\sqrt{2\Delta} \qquad \text{Eq.2.2.}$$

where relative refractive index is defined as:

$$\Delta = \frac{n_1^2 - n_0^2}{2n_1^2} \cong \frac{n_1 - n_0}{n_1} \qquad \text{Eq.2.3.}$$

2.1.1. Formation of Modes:

Although entrance angle φ can be an interval of numerical aperture, the rays inside the optical fiber cannot propagate at arbitrary angles. Each mode is associated with a special angle of propagation. The propagation of light inside optical fiber is demonstrated in Fig. 2.2.

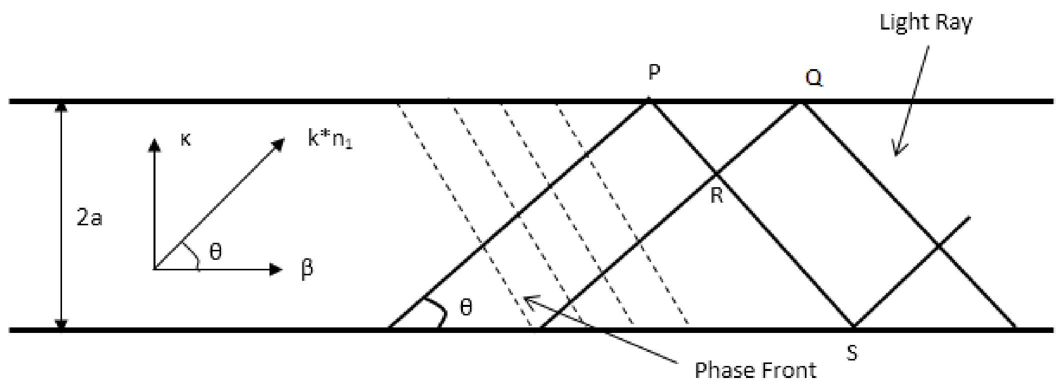

Figure 2.2. Propagation of light ray and phase front of mode inside optical fiber

The wavelength in the core is λ_0/n_2 where λ_0 is the free space wavelength and the correspnding wave number is k_0*n_2 where k_0 is the free space wave number. The wave number has two components: longtitutional(β) and transverse(κ) components. These two components of wave numbers are expressed by

$$\beta = k_0 * n_1 * \cos\theta \qquad \text{Eq.2.4.a}$$

$$\kappa = k_0 * n_1 * \sin\theta \qquad \text{Eq.2.4.b}$$

Consider two plane waves are in the same waveguide with having phase difference between them. The ray that moves from R to Q (RQ) does not suffer from reflection. The light ray moves from P to S (PS) reflects two times. Since RQ and PS are in the same phase front, the optical path differences should be multiple of 2π. The reflection coefficient of totally reflected from core-cladding interface is expressed:

$$r = \frac{A_r}{A_i} = \frac{n_1 \sin\theta + i\sqrt{n_1^2 \cos\theta^2 - n_0^2}}{n_1 \sin\theta - i\sqrt{n_1^2 \cos\theta^2 - n_0^2}} \qquad \text{Eq.2.5}$$

The reflection coefficient also is explained as r = exp[-i*Φ] where Φ is the amount of phase shift during reflection. The phase shift is calculated from Eq.2.5:

$$\Phi = -2 * \tan^{-1} \frac{\sqrt{n_1^2 \cos\theta^2 - n_0^2}}{n_1 \sin\theta} \qquad \text{Eq.2.6.}$$

The distance between points Q and R is

$$\frac{2a}{\tan\theta} - 2a * \tan\theta \qquad \text{Eq.2.7.}$$

The distance between P and Q is expressed as:

$$l_1 = (\frac{2a}{\tan\theta} - 2a * \tan\theta) \cos\theta = \frac{2a}{\sin\theta} - 2a * \sin\theta \qquad \text{Eq.2.8.}$$

The distance between R and S is expressed as:

$$l_2 = \frac{2a}{\sin\theta} \qquad \text{Eq.2.9.}$$

Applying the phase matching condition for the optical paths PQ and RS results in:

$$(k_0 * n_1 * l_2 + 2\Phi) - k_0 * n_1 * l_1 = 2 * m * \pi \qquad \text{Eq.2.10.}$$

where m is integer numbers. Then, after Eq.2.6, Eq. 2.8 and Eq.2.9 are inserted into Eq.2.10, then we get condition for propagation.

$$\tan^{-1}\left((k_0 * n_1 * a * \sin\theta - m\frac{\pi}{2}\right) = \sqrt{\frac{2\Delta}{\sin\theta^2} - 1} \qquad \text{Eq.2.11.}$$

Eq.2.11 shows that the propagation angle of a wave inside optical fibers is discrete. This angle depends on the waveguide structure (core radius a, the refractive indices of core and cladding) and wave number of propagating light.

The optical field distribution that satisfies this condition is called as mode. The mode m= 0 corresponds the fundamental mode. The number increases until θ reaches the critical angle for the total internal reflection.

2.2. The Field Calculations:

Helmholtz equation in cylindrical coordinates is used for solving mode fields present in fibers.

$$\frac{1}{r}\frac{\partial}{\partial r}\left(r\frac{\partial \psi}{\partial r}\right)+\frac{1}{r^2}\frac{\partial^2 \psi}{\partial \theta^2}+\frac{\partial^2 \psi}{\partial z^2}+k^2\psi=0 \qquad \text{Eq.2.12.}$$

Electric and magnetic fields propagating in z direction in cylindrical waveguides are expressed as:

$$\vec{E}=E(r,\theta)e^{-i(\omega t-\beta z)} \qquad \text{Eq.2.13.a}$$

$$\vec{H}=H(r,\theta)e^{-i(\omega t-\beta z)} \qquad \text{Eq.2.13.b}$$

If above electric and magnetic field equations are inserted to Helmholtz equation, we obtain wave equations for electric and magnetic fields.

$$\frac{\partial^2 E_z}{\partial r^2}+\frac{1}{r}\frac{\partial E_z}{\partial r}+\frac{1}{r^2}\frac{\partial^2 E_z}{\partial \theta^2}+\left[k^2n(r,\theta)^2-\beta^2\right]E_z=0 \qquad \text{Eq.2.14.a.}$$

$$\frac{\partial^2 H_z}{\partial r^2}+\frac{1}{r}\frac{\partial H_z}{\partial r}+\frac{1}{r^2}\frac{\partial^2 H_z}{\partial \theta^2}+\left[k^2n(r,\theta)^2-\beta^2\right]H_z=0 \qquad \text{Eq.2.14.b.}$$

The transverse field components in terms of E_z and H_z are expressed as:

$$E_r=\frac{-i}{\left[k^2n(r,\theta)^2-\beta^2\right]}\left(\beta\frac{\partial E_z}{\partial r}+\frac{\omega\mu_0}{r}\frac{\partial H_z}{\partial \theta}\right) \qquad \text{Eq.2.15.a}$$

$$E_\theta=\frac{-i}{\left[k^2n(r,\theta)^2-\beta^2\right]}\left(\frac{\beta}{r}\frac{\partial E_z}{\partial \theta}+\omega\mu_0\frac{\partial H_z}{\partial r}\right) \qquad \text{Eq.2.15.b}$$

$$H_r = \frac{-i}{[k^2n(r,\theta)^2 - \beta^2]}(\beta\frac{\partial H_z}{\partial r} + \frac{\omega\mu_0 n(r)^2}{r}\frac{\partial E_z}{\partial \theta}) \qquad \text{Eq.2.15.c}$$

$$H_\theta = \frac{-i}{[k^2n(r,\theta)^2 - \beta^2]}(\frac{\beta}{r}\frac{\partial H_z}{\partial \theta} + \omega\mu_0 n(r)^2\frac{\partial E_z}{\partial r}) \qquad \text{Eq.2.15.d}$$

In terms of polarization, there are 3 different modes in cylindrical waveguides: TE modes ($E_z = 0$), TM modes ($H_z = 0$) and hybrid modes ($E_z \neq 0$, $H_z \neq 0$).

2.2.1. TE Modes:

In TE modes, transverse electric field in direction of propagation is zero. ($E_z = 0$). Therefore, we have wave equation for TE mode:

$$\frac{\partial^2 H_z}{\partial r^2} + \frac{1}{r}\frac{\partial H_z}{\partial r} + \frac{1}{r^2}\frac{\partial^2 H_z}{\partial \theta^2} + [k^2n(r,\theta)^2 - \beta^2]\, H_z = 0 \qquad \text{Eq.2.16}$$

The transverse electromagnetic fields are expressed as

$$E_r = \frac{-i}{[k^2n(r,\theta)^2 - \beta^2]}\frac{\omega\mu_0}{r}\frac{\partial H_z}{\partial \theta} \qquad \text{Eq.2.17.a}$$

$$E_\theta = \frac{-i\omega\mu_0}{[k^2n(r,\theta)^2 - \beta^2]}\frac{\partial H_z}{\partial r}) \qquad \text{Eq.2.17.b}$$

$$H_r = \frac{-i\beta}{[k^2n(r,\theta)^2 - \beta^2]}\frac{\partial H_z}{\partial r} \qquad \text{Eq.2.17.c}$$

$$H_\theta = \frac{-i}{[k^2n(r,\theta)^2 - \beta^2]}\frac{\beta}{r}\frac{\partial H_z}{\partial \theta} \qquad \text{Eq.2.17.d}$$

Magnetic field in the direction of propagation is expressed as

$$\mathrm{H_z} = \begin{cases} \mathrm{g(r)} * \cos(n\theta + \varphi), & 0 \leq \mathrm{x} \leq \mathrm{a} \\ \mathrm{h(r)} * \sin(n\theta + \varphi), & \mathrm{r} > \mathrm{a} \end{cases} \qquad \text{Eq.2.18}$$

From the boundary condition, the wave fields at core-cladding interface should be continuous. Therefrore we get two equalities:

$$\mathrm{g(a) = h(a)} \qquad \text{Eq.2.19.a}$$

$$\frac{-i\beta}{[k^2n(r,\theta)^2-\beta^2]}\frac{n}{a}g(a)\sin(n\theta+\varphi) = \frac{-i\beta}{[k^2n(r,\theta)^2-\beta^2]}\frac{n}{a}h(a)\sin(n\theta+\varphi) \quad \text{Eq.2.19.b}$$

n(a) is the refractive index of the core. In order to match the condition the propagation of modes that explained in Eq.2.11., propagation angles θ take arbitrary values and n becomes 0. As n equals to 0, $\partial/\partial\theta$ goes to 0. Therefore, $E_z = H_\theta = 0$. After this expressions, the wave equation becomes

$$\frac{\partial^2 H_z}{\partial r^2}+\frac{1}{r}\frac{\partial H_z}{\partial r}+[k^2n(r)^2-\beta^2]\,H_z=0 \quad \text{Eq.2.20}$$

We can define two wavenumbers along transversal direction inside the fiber:

$$\kappa=\sqrt{n_1^2k_0^2-\beta^2} \quad \text{Eq.2.21.a}$$

$$\sigma=\sqrt{\beta^2-n_0^2k_0^2} \quad \text{Eq.2.21.b}$$

where κ is transverse wavenumber in the core and σ is transverse wavenumber in the cladding.

Magnetic field in the core (H_z = g(r)) can be expressed as:

$$\frac{d^2g}{dr^2}+\frac{1}{r}\frac{dg}{dr}+\kappa^2 g=0 \quad \text{Eq.2.22}$$

The solutions for Eq.2.22 are 0^{th} order Bessel function J(κr) and Neumann function N(κr) for above solution. However, Neumann function diverges infinity at r = 0. Therefore, 0^{th} order Bessel function is proper solution. Magnetic field in the cladding (H_z = h(r)) can be expressed as:

$$\frac{d^2h}{dr^2}+\frac{1}{r}\frac{dh}{dr}+\sigma^2 g=0 \quad \text{Eq.2.23}$$

The solutions for Eq.2.23 Modified Bessel function of first kind $I_0(\sigma r)$ and Modified Bessel function of second kind $K_0(\sigma r)$. Because $I_0(\sigma r)$ diverges to infinity at r = ∞, $K_0(\sigma r)$ is the proper solution for radial component in cladding. Therefore, the radial components of the magnetic fields in core and cladding are expressed as:

$$\mathrm{H_z} = \begin{cases} \mathrm{A} * J_0(\kappa * r), & 0 \le \mathrm{x} \le \mathrm{a} \\ \mathrm{B} * K_0(\sigma * r), & \mathrm{r} > \mathrm{a} \end{cases} \qquad \text{Eq.2.24}$$

The boundary conditions at core-cladding interface are reduced to

$$\mathrm{A} * J_0(\kappa * a) = \mathrm{B} * K_0(\sigma * a) \qquad \text{Eq.2.25.a}$$

$$\frac{A}{\kappa} J_0'(\kappa * a) = -\frac{B}{\sigma} K_0'(\sigma * a) \qquad \text{Eq.2.25.b}$$

By using normalized transverse parameters

$$\mathrm{u} = \kappa * a = a\sqrt{n_1^2 k_0^2 - \beta^2} \qquad \text{Eq.2.26.a}$$

$$\mathrm{w} = \sigma * a = a\sqrt{\beta^2 - n_0^2 k_0^2} \qquad \text{Eq.2.26.b}$$

Eq.2.25.a and Eq.2.25.b reduces to following relation:

$$\frac{J_0'(u)}{u * J_0(u)} = -\frac{K_0'(w)}{w * K_0(w)} \qquad \text{Eq.2.27.}$$

Inserting following Bessel formulation into Eq. 2.27:

$$J_0'(u) = -J_1(u) \qquad \text{Eq.2.28.a}$$

$$K_0'(w) = -K_1(w) \qquad \text{Eq.2.28.b}$$

We obtain a new relation:

$$\frac{J_1(u)}{u * J_0(u)} = -\frac{K_1(w)}{w * K_0(w)} \qquad \text{Eq.2.29.}$$

The parameters u and w are related as

$$u^2 + w^2 = k_0^2(n_1^2 - n_0^2)a^2 = V^2 \qquad \text{Eq.2.30}$$

The parameter V is called as normalized frequency. Inserting normalized parameter into Eq. 2.29, the transverse wavenumbers for core (u) and cladding (w) can be founded. The TE wave fields in core and cladding are expressed as

$$E_z = E_r = H_\theta \qquad \text{Eq.2.31.}$$

Fields in the core:

$$E_\theta = i\omega\mu_0 \frac{a}{u} A J_1(\frac{u}{a} r) \qquad \text{Eq.2.32.a}$$

$$H_r = -i\beta \frac{a}{u} A J_1(\frac{u}{a} r) \qquad \text{Eq.2.32.b}$$

$$H_z = AJ_0(\frac{u}{a}r) \qquad \text{Eq.2.32.c}$$

Fields in the cladding:

$$E_\theta = i\omega\mu_0 \frac{a}{w}\frac{J_0(u)}{K_0(w)} AJ_1(\frac{w}{a}r) \qquad \text{Eq.2.32.a}$$

$$H_r = -i\beta \frac{a}{w}\frac{J_0(u)}{K_0(w)} AJ_1(\frac{w}{a}r) \qquad \text{Eq.2.32.b}$$

$$H_z = A\frac{J_0(u)}{K_0(w)} J_0(\frac{w}{a}r) \qquad \text{Eq.2.32.c}$$

The coefficient A is related with laser intensity. It is taken as unity in the calculations.

2.2.2. TM Modes:

In TM modes, transverse electric field in direction of propagation is zero ($H_z = 0$). The azimuthal parameter (n) is equal to zero. The wave equation and related transverse field equations are written as:

$$\frac{\partial^2 E_z}{\partial r^2} + \frac{1}{r}\frac{\partial E_z}{\partial r} + \frac{1}{r^2}\frac{\partial^2 E_z}{\partial \theta^2} + [k^2 n(r,\theta)^2 - \beta^2]\, E_z = 0 \qquad \text{Eq.2.33}$$

$$E_r = \frac{-i\beta}{[k^2 n(r,\theta)^2 - \beta^2]}\frac{\partial E_z}{\partial r} \qquad \text{Eq.2.34.a}$$

$$E_\theta = \frac{-i}{[k^2 n(r,\theta)^2 - \beta^2]}\frac{\beta}{r}\frac{\partial E_z}{\partial \theta} \qquad \text{Eq.2.34.b}$$

$$H_r = \frac{-i}{[k^2 n(r,\theta)^2 - \beta^2]}\frac{\omega\mu_0 n(r)^2}{r}\frac{\partial E_z}{\partial \theta} \qquad \text{Eq.2.34.c}$$

$$H_\theta = \frac{-i\omega\mu_0 n(r)^2}{[k^2 n(r,\theta)^2 - \beta^2]}\frac{\partial E_z}{\partial r} \qquad \text{Eq.2.34.d}$$

The solution of wave equation Eq. 2.33 that gives radial component of wave field is expressed as:

$$\mathrm{E_z} = \begin{cases} \mathrm{A} * J_0(\kappa * r), & 0 \le \mathrm{x} \le \mathrm{a} \\ \mathrm{B} * K_0(\sigma * r), & \mathrm{r} > \mathrm{a} \end{cases} \qquad \text{Eq.2.35}$$

Applying boundary conditions that E_z and H_θ are both continuous at core-cladding interface then,

$$\frac{J_0'(u)}{u * J_0(u)} = -(\frac{n_0}{n_1})^2 \frac{K_0'(w)}{w * K_0(w)} \qquad \text{Eq.2.36}$$

If Bessel relations in Eq. 2.28.a and 2.28.b are inserted into Eq. 2.36, then above dispersion relation for TM modes becomes

$$\frac{J_1(u)}{u * J_0(u)} = -(\frac{n_0}{n_1})^2 \frac{K_1(w)}{w * K_0(w)} \qquad \text{Eq.2.37}$$

As n equals to zero, $\partial/\partial\theta$ becomes zero like calculation in TE modes. Then, the electromagnetic fields of TM modes are expressed as

$$H_z = H_r = E_\theta \qquad \text{Eq.2.38.}$$

Fields in the core:

$$E_r = i\beta \frac{a}{u} A J_1(\frac{u}{a} r) \qquad \text{Eq.2.39.a}$$

$$H_\theta = -i\omega\varepsilon_0 n_1^2 \frac{a}{u} A J_1(\frac{u}{a} r) \qquad \text{Eq.2.39.b}$$

$$E_z = A J_0(\frac{u}{a} r) \qquad \text{Eq.2.39.c}$$

Fields in the cladding:

$$E_r = i\beta \frac{J_0(u)}{K_0(w)} A J_1(\frac{w}{a} r) \qquad \text{Eq.2.40.a}$$

$$H_\theta = -i\omega\varepsilon_0 n_1^2 \frac{J_0(u)}{K_0(w)} A J_1(\frac{w}{a} r) \qquad \text{Eq.2.40.b}$$

$$E_z = A \frac{J_0(u)}{K_0(w)} J_0(\frac{w}{a} r) \qquad \text{Eq.2.40.c}$$

2.2.3. Hybrid Modes:

In hybrid modes, axial components of electromagnetic fields E_z and H_z are not equal to zero. Therefore, the solution have components of n-th order Bessel function in radial direction and cos(nθ + φ) or sin(nθ + φ) in azimuthal direction. E_z and H_z are both continuous at r =a. The z-components of the electromagnetic field are expressed as

$$E_z = \begin{cases} AJ_n(\frac{u}{a}r)\cos(n\theta+\varphi), & 0<r<a \\ A\frac{J_n(u)}{K_n(w)_n}K_n(\frac{w}{a}r)\cos(n\theta+\varphi), & r\geq a \end{cases}$$ Eq.2.41.a Eq.2.41.b

$$H_z = \begin{cases} AJ_n(\frac{u}{a}r)\sin(n\theta+\varphi), & 0<r<a \\ A\frac{J_n(u)}{K_n(w)_n}K_n(\frac{w}{a}r)\sin(n\theta+\varphi), & r\geq a \end{cases}$$ Eq.2.42.a Eq.2.42.b

The transverse core fields are written as by substituting Eq 2.41 and 2.42 into Eq. 2.15:

Fields in the core:

$$E_r = -\frac{ia^2}{u^2}[A\beta\frac{u}{a}J_n'\left(\frac{u}{a}r\right) + C\omega\mu_0\frac{n}{r}J_n\left(\frac{u}{a}r\right)]\ \cos(n\theta+\ \varphi)$$ Eq.2.43.a

$$E_\theta = -\frac{ia^2}{u^2}[-A\beta\frac{n}{r}J_n\left(\frac{u}{a}r\right) - C\omega\mu_0\frac{u}{a}J_n'\left(\frac{u}{a}r\right)]\ \sin(n\theta+\ \varphi)$$ Eq.2.43.b

$$H_r = -\frac{ia^2}{u^2}[A\omega\varepsilon_0 n_1^2 J_n\left(\frac{u}{a}r\right) + C\beta\frac{u}{a}J_n'\left(\frac{u}{a}r\right)]\ \sin(n\theta+\ \varphi)$$ Eq.2.43.c

$$H_\theta = -\frac{ia^2}{u^2}[A\omega\varepsilon_0 n_1^2\frac{u}{a}J_n'\left(\frac{u}{a}r\right) + C\beta\frac{n}{r}J_n\left(\frac{u}{a}r\right)]\ \cos(n\theta+\ \varphi)$$ Eq.2.43.d

Fields in the cladding:

$$E_r = \frac{ia^2}{w^2}[A\beta\frac{w}{a}K_n'\left(\frac{w}{a}r\right) + C\omega\mu_0\frac{n}{r}K_n\left(\frac{w}{a}r\right)]\frac{J_n(u)}{K_n(w)}\ \cos(n\theta+\ \varphi)$$ Eq.2.44.a

$$E_\theta = \frac{ia^2}{w^2}[-A\beta\frac{n}{r}K_n\left(\frac{w}{a}r\right) - C\omega\mu_0\frac{w}{a}K_n'\left(\frac{w}{a}r\right)]\frac{J_n(u)}{K_n(w)}\ \sin(n\theta+\ \varphi)$$ Eq.2.44.b

$$H_r = \frac{ia^2}{w^2}[A\omega\varepsilon_0 n_1^2 K_n\left(\frac{w}{a}r\right) + C\beta\frac{w}{a}K_n'\left(\frac{w}{a}r\right)]\frac{J_n(u)}{K_n(w)}\ \sin(n\theta+\ \varphi)$$ Eq.2.44.c

$$H_\theta = \frac{ia^2}{w^2}[A\omega\varepsilon_0 n_1^2 \frac{w}{a} K_n'\left(\frac{w}{a}r\right) + C\beta \frac{n}{r} K_n\left(\frac{w}{a}r\right)] \frac{J_n(u)}{K_n(w)} \cos(n\theta + \varphi) \qquad \text{Eq.2.44.d}$$

E_θ and H_θ should be continuous to get the continuity at r = a. If 2.43.b and 2.44.b are equalized at r =a, first relation can be obtained:

$$A\beta\left(\frac{1}{u^2} + \frac{1}{w^2}\right)n = -C\omega\mu_0\left(\frac{J_n'(u)}{u * J_n(u)} + \frac{K_n'(w)}{w * K_n(w)}\right) \qquad \text{Eq.2.45}$$

If 2.43.d and 2.44.d are equalized at r =a, second relation can be obtained:

$$A\omega\varepsilon_0\left[n_1^2 \frac{J_n'(u)}{u * J_n(u)} + n_0^2 \frac{K_n'(w)}{w * K_n(w)}\right] = -C\beta\left(\frac{1}{u^2} + \frac{1}{w^2}\right)n \qquad \text{Eq.2.46}$$

The generalized dispersion equation is obtained by combining Eq.2.45 and Eq.2.46.

$$\left[\frac{J_n'(u)}{u * J_n(u)} + \frac{K_n'(w)}{w * K_n(w)}\right]\left[n_1^2 \frac{J_n'(u)}{u * J_n(u)} + n_0^2 \frac{K_n'(w)}{w * K_n(w)}\right] = \frac{\beta^2}{k^2}\left(\frac{1}{u^2} + \frac{1}{w^2}\right)n^2 \qquad \text{Eq.2.47}$$

Using normalized frequency relation for optical fiber in Eq 2.30,

$$\frac{\beta^2}{k^2}\left(\frac{1}{u^2} + \frac{1}{w^2}\right)n^2 = \frac{n_1^2}{u^2} + \frac{n_0^2}{w^2} \qquad \text{Eq.2.48}$$

Then, Eq. 2.48 can be rewritten as

$$\left[\frac{J_n'(u)}{u * J_n(u)} + \frac{K_n'(w)}{w * K_n(w)}\right]\left[\frac{J_n'(u)}{u * J_n(u)} + \frac{n_0^2}{n_1^2}\frac{K_n'(w)}{w * K_n(w)}\right] = \left(\frac{1}{u^2} + \frac{1}{w^2}\right)n^2\left(\frac{1}{u^2} + \frac{n_0^2}{n_1^2}\frac{1}{w^2}\right) \qquad \text{Eq.2.49}$$

Above relation is used to calculate propagation constants of hybrid modes by using u-w relation in Eq. 1.26. The constant C in the electromagnetic field expressions is that

$$C = -A\frac{\beta}{\omega\mu_0}s \qquad \text{Eq.2.50}$$

where parameter s equals to

$$s = \frac{(\frac{1}{u^2} + \frac{1}{w^2})n}{\left[\frac{J_n'(u)}{u * J_n(u)} + \frac{K_n'(w)}{w * K_n(w)}\right]} \qquad \text{Eq.2.51}$$

Applying following Bessel relations:

$$J_n'(z) = \frac{1}{2}[J_{n-1}(z) - J_{n+1}(z)] \qquad \text{Eq.2.52.a}$$

$$\frac{n}{z}J_n(z) = \frac{1}{2}[J_{n-1}(z) + J_{n+1}(z)] \qquad \text{Eq.2.52.b}$$

$$K_n'(z) = \frac{1}{2}[K_{n-1}(z) - K_{n+1}(z)] \qquad \text{Eq.2.52.c}$$

$$\frac{n}{z}K_n(z) = \frac{1}{2}[K_{n-1}(z) + K_{n+1}(z)] \qquad \text{Eq.2.52.d}$$

Then, Eq.2.41-Eq.2.44 becomes

Fields in the core:

$$E_r = -iA\beta\frac{a}{u}[\frac{1-s}{2}J_{n-1}\left(\frac{u}{a}r\right) - \frac{1+s}{2}J_{n+1}\left(\frac{u}{a}r\right)]\cos(n\theta + \varphi) \qquad \text{Eq.2.53.a}$$

$$E_\theta = -iA\beta\frac{a}{u}[\frac{1-s}{2}J_{n-1}\left(\frac{u}{a}r\right) - \frac{1+s}{2}J_{n+1}\left(\frac{u}{a}r\right)]\sin(n\theta + \varphi) \qquad \text{Eq.2.53.b}$$

$$E_z = AJ_n\left(\frac{u}{a}r\right)\cos(n\theta + \varphi) \qquad \text{Eq.2.53.c}$$

$$H_r = -iA\omega\varepsilon_0 n_1^2\frac{a}{u}[\frac{1-s_1}{2}J_{n-1}\left(\frac{u}{a}r\right) - \frac{1+s_1}{2}J_{n+1}\left(\frac{u}{a}r\right)]\sin(n\theta + \varphi) \qquad \text{Eq.2.53.d}$$

$$H_\theta = -iA\omega\varepsilon_0 n_1^2\frac{a}{u}[\frac{1-s_1}{2}J_{n-1}\left(\frac{u}{a}r\right) - \frac{1+s_1}{2}J_{n+1}\left(\frac{u}{a}r\right)]\sin(n\theta + \varphi) \qquad \text{Eq.2.53.e}$$

$$H_z = -A\frac{\beta}{\omega\mu_0}sJ_n\left(\frac{u}{a}r\right)\sin(n\theta + \varphi) \qquad \text{Eq.2.53.f}$$

Fields in the cladding:

$$E_r = -iA\beta \frac{aJ_n(u)}{wK_n(w)}[\frac{1-s}{2}K_{n-1}\left(\frac{w}{a}r\right) - \frac{1+s}{2}K_{n+1}\left(\frac{w}{a}r\right)]\cos(n\theta + \varphi) \qquad \text{Eq.2.53.a}$$

$$E_\theta = -iA\beta \frac{aJ_n(u)}{wK_n(w)}[\frac{1-s}{2}K_{n-1}\left(\frac{w}{a}r\right) - \frac{1+s}{2}K_{n+1}\left(\frac{w}{a}r\right)]\sin(n\theta + \varphi) \qquad \text{Eq.2.53.b}$$

$$E_z = AJ_n \frac{J_n(u)}{K_n(w)}\left(\frac{u}{a}r\right)\cos(n\theta + \varphi) \qquad \text{Eq.2.53.c}$$

$$H_r = -iA\omega\varepsilon_0 n_1^2 \frac{aJ_n(u)}{wK_n(w)}[\frac{1-s_1}{2}K_{n-1}\left(\frac{w}{a}r\right) - \frac{1+s_1}{2}K_{n+1}\left(\frac{w}{a}r\right)]\sin(n\theta + \varphi) \qquad \text{Eq.2.53.d}$$

$$H_\theta = -iA\omega\varepsilon_0 n_1^2 \frac{aJ_n(u)}{wK_n(w)}[\frac{1-s_1}{2}K_{n-1}\left(\frac{w}{a}r\right) - \frac{1+s_1}{2}K_{n+1}\left(\frac{w}{a}r\right)]\sin(n\theta + \varphi) \qquad \text{Eq.2.53.e}$$

$$H_z = -A\frac{\beta}{\omega\mu_0}\frac{J_n(u)}{K_n(w)}sK_n\left(\frac{w}{a}r\right)\sin(n\theta + \varphi) \qquad \text{Eq.2.53.f}$$

where

$$s_1 = \frac{\beta^2}{k^2 n_1^2}s \qquad \text{Eq.2.54.a}$$

$$s_0 = \frac{\beta^2}{k^2 n_0^2}s \qquad \text{Eq.2.54.b}$$

2.3. Linearly Polarized Modes:

In previous sections, TM, TE and hybrid modes have been analyzed. The refractive index difference (Δn) of the commercial fibers is around 1%. Due to small amount of refractive index difference, it can be approximated as $n_1/n_0 \approx 1$. This approximation was firstly made by Snitzer[71] and designated as LP (linearly polarized) modes by Gloge[72]. LP modes are designated as LP_{ml} where m is the azimuthal and l is the radial parameter.

These LP modes are the superpositions of the TE, TM and hybrid modes. Applying this approximation to three polarizations, the dispersion equation for LP modes can be expressed as

$$\frac{J_{m+1}(u)}{u * J_m(u)} = -\frac{K_{m+1}(w)}{wK_m(w)} \qquad \text{Eq.2.55}$$

If we modify Eq.2.56 by using Eq.2.30, we get a new relation

$$-\frac{u * K_{m+1}\left(\sqrt{V^2 - u^2}\right) * J_m(u)}{J_{m+1}(u) * K_m\left(\sqrt{V^2 - u^2}\right)} = \sqrt{V^2 - u^2} \qquad \text{Eq.2.56}$$

By solving Eq.2.56 with graphical method, we can find transverse propagation parameters of the modes.

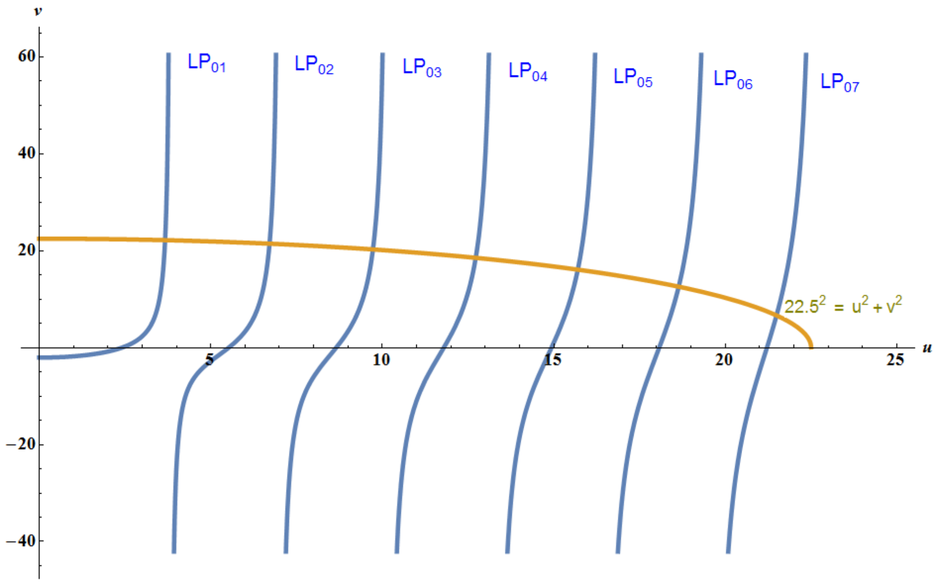

Figure 2.3. Graphical construction for solving Eq.2.57 with m = 0 and V = 22.5.

In Fig.2.3, the intersection points of blue lines and olive line gives the normalized transverse parameters for propagating waves in the core (u parametter). These two lines indicates the left hand side and right hand side of the Eq.2.56. From Eq.2.30, to find the transverse κ and longitutional β parameters, the propagation characteristics of each mode can be understood. The V-number is for a waveguide that has 25 μm core radius with NA = 0.22 and 1550 nm coherent source.

For every value of m, at least one solution exist for Eq.2.56. As the m increses, the number of solutions decreases. The solution must be lover than V-number of the waveguide.

The electromagnetic field distributions of LP modes inside of optical fibers are expressed as

Fields in the core:

$$E_r = -iA\beta \frac{a}{u} [J_{n-1}\left(\frac{u}{a}r\right) - J_{n+1}\left(\frac{u}{a}r\right)] \cos(n\theta + \varphi) \qquad \text{Eq.2.57.a}$$

$$E_\theta = iA\beta \frac{a}{u} [\frac{1-s}{2} J_{n-1}\left(\frac{u}{a}r\right) + \frac{1+s}{2} J_{n+1}\left(\frac{u}{a}r\right)] \sin(n\theta + \varphi) \qquad \text{Eq.2.57.b}$$

$$E_z = AJ_n\left(\frac{u}{a}r\right) \cos(n\theta + \varphi) \qquad \text{Eq.2.57.c}$$

$$H_r = -iA\omega\varepsilon_0 n_1^2 \frac{a}{u} [J_{n-1}\left(\frac{u}{a}r\right) - J_{n+1}\left(\frac{u}{a}r\right)] \sin(n\theta + \varphi) \qquad \text{Eq.2.57.d}$$

$$H_\theta = -iA\omega\varepsilon_0 n_1^2 \frac{a}{u} [J_{n-1}\left(\frac{u}{a}r\right) + J_{n+1}\left(\frac{u}{a}r\right)] \cos(n\theta + \varphi) \qquad \text{Eq.2.57.e}$$

$$H_z = -A\frac{\beta}{\omega\mu_0} J_n\left(\frac{u}{a}r\right) \sin(n\theta + \varphi) \qquad \text{Eq.2.57.f}$$

Fields in the cladding:

$$E_r = -iA\beta \frac{aJ_n(u)}{wK_n(w)} [K_{n-1}\left(\frac{w}{a}r\right) - K_{n+1}\left(\frac{w}{a}r\right)] \cos(n\theta + \varphi) \qquad \text{Eq.2.58.a}$$

$$E_\theta = iA\beta \frac{aJ_n(u)}{wK_n(w)} [\frac{1-s}{2} K_{n-1}\left(\frac{w}{a}r\right) + \frac{1+s}{2} K_{n+1}\left(\frac{w}{a}r\right)] \sin(n\theta + \varphi) \qquad \text{Eq.2.58.b}$$

$$E_z = A\frac{J_n(u)}{K_n(w)} K_n\left(\frac{w}{a}r\right) \cos(n\theta + \varphi) \qquad \text{Eq.2.58.c}$$

$$H_r = -iA\omega\varepsilon_0 n_1^2 \frac{aJ_n(u)}{wK_n(w)} [K_{n-1}\left(\frac{w}{a}r\right) - K_{n+1}\left(\frac{w}{a}r\right)] \sin(n\theta + \varphi) \qquad \text{Eq.2.58.d}$$

$$H_\theta = -iA\omega\varepsilon_0 n_1^2 \frac{aJ_n(u)}{wK_n(w)}[K_{n-1}\left(\frac{w}{a}r\right) + K_{n+1}\left(\frac{w}{a}r\right)]\cos(n\theta + \varphi) \qquad \text{Eq.2.58.e}$$

$$H_z = -A\frac{\beta}{\omega\mu_0}\frac{J_n(u)}{K_n(w)}K_n\left(\frac{w}{a}r\right)\sin(n\theta + \varphi) \qquad \text{Eq.2.58.f}$$

Throughout the thesis, field and intensity calculations are made by using E_z component of the core and cladding fields (Eq.2.58.c and Eq.2.59.c). Fig.2.4 shows calculation of the intensity of some modes present in the 25-µm core radius optical fibers.

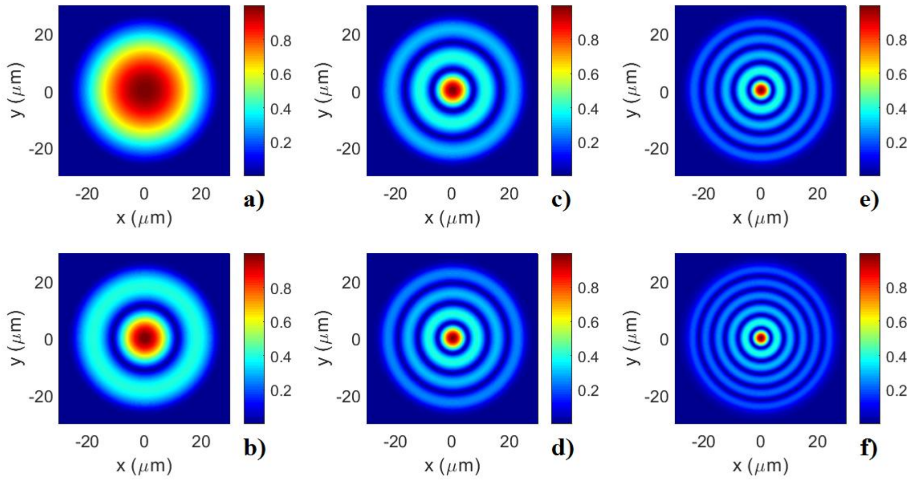

Figure 2.4. Intensity profiles of present modes a) LP_{01}, b) LP_{02}, c) LP_{03}, d) LP_{04}, e) LP_{05}, f) LP_{06} in optical fibers with V =22.5

In Fig. 2.4, it is shown that as the as the radial index l increases, there are rings formed and intensity in the center of the is distributed through core-cladding interface. The number of formed rings are equal to radial parameter of the LP mode.

2.4. Theory of Wavefront Shaping:

The propagation of any input field (E_{in}) through a fiber of length L, causing the output field E_{out} can be explained by[73]

$$E_{out}(x,y) = \sum_{n=1}^{\#\,Modes} \alpha_n E_n(x,y)e^{-i\beta_n L} \qquad \text{Eq.2.60}$$

where E_n is the normalized LP-mode profile and α_n is the cross-correlation between the normalized n^{th} mode and the input field, given by:

$$\alpha_n = \int\int E_{in}(x,y)E_n^*(x,y)dydx \qquad \text{Eq.2.61}$$

Eq.2.60 is the main equation for wavefront shaping. By controlling input wave field, the desired output can be obtained. In wavefront shaping experiments, the phase mask is programmed on the SLM screen. Liquid crystals on the SLM introduce additional optical length. This causes phase change of light. Depending on the application, The total transmission of medium can be increased[75] or an opaque lens in a scattering medium can be created[19] by programming SLM.

In our calculations, the phases between 0 and 2π are assigned to modes in order to control and manipulation of light inside the fiber.

CHAPTER III

RESULTS

In this chapter, we provide calculation results on mode profiles inside multimode fibers. We investigate the effect of the multimode core radius on speckle patterns that are formed at the output facet. In our calculations, we control the relative phase of the modes to get optimized intensity patterns. As a result, we are able to increase to transmission through the fiber as well as focusing light to create a single spot. We establish a method to perform optical modulation of light through fiber by controlling a selected mode. We also investigate the response of the speckle patterns as well as the optimized fiber output patterns at different input frequencies. We observe that the output speckle patterns are more sensitive to input frequencies when the core radius is increased.

3.1. Speckle Patterns at Output of the Optical Fiber:

In this section, we investigate the speckle patterns at various fiber core radius settings. We perform calculations at an input wavelength of $\lambda = 1.55$ µm, numerical aperture of the fiber NA = 0.22, fiber length with 10 cm and at various core radii. In our calculations, we do not take dispersion into account. Most of calculations are perfromed for a bandwidth of $\Delta\lambda = 4$ nm within the transparency window of telecom fibers where dispersion is neglicible.

The speckle pattern is obtained by interference of all supported modes at the ouput facet of the optical fiber with both core and cladding field calculations. In these calculations the effect of noise and mode coupling is neglected. For mode calculations, the Eq.2.58.c and Eq.2.59.c are used for field calculations. In addition to these equations, the propagation in the z direction to the equations is added. Therefore, above equations become

$$E_z = \begin{cases} AJ_n\left(\frac{u}{a}r\right)\cos(n\theta + \varphi), & x < 0 \quad \text{Eq.4.1.a} \\ A\frac{J_n(u)}{K_n(w)}K_n\left(\frac{w}{a}r\right)\cos(n\theta + \varphi), & x \geq 0 \quad \text{Eq.4.1.b} \end{cases}$$

Table 3.1. The change of V-number and number of modes size with changing radius of core of optical fibers

Core Radius (µm)	V-Number	Number of Modes
5	4.459	4
10	8.918	13
25	22.295	68
50	44.59	258
100	89.18	1021
200	178.36	4055

As it is shown from Figure.3.1, as the number of normalized frequency increases, both number and intensity of peaks in the outputs increases. We can see speckles 25-50-100-200 µm core radius fiber because the number modes in the waveguide increases and the interference of these modes creates more complex pattern. Also, with increasing core radius, the number of spots increases.

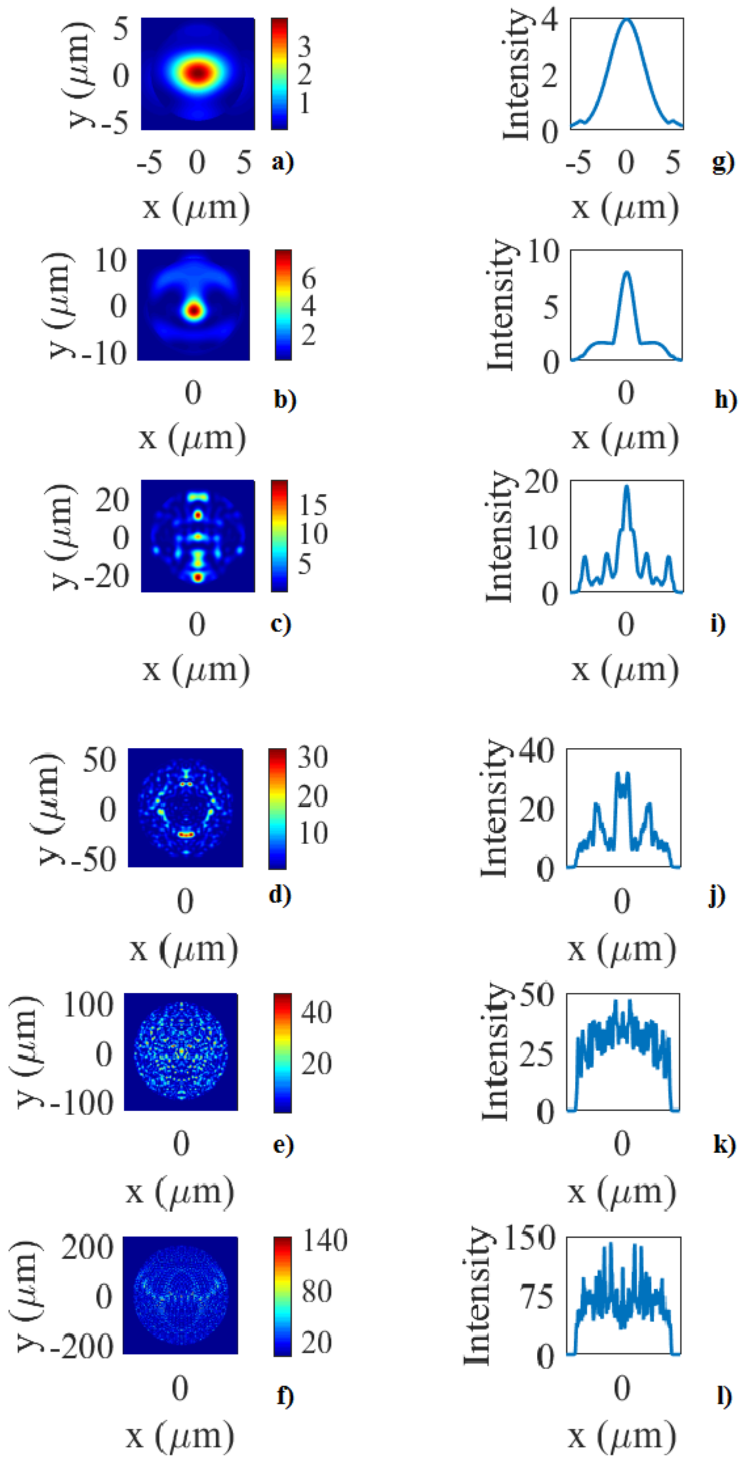

Figure 3.1. Calculated speckle pattern for a core radius of (a) 5 μm, (b) 10 μm, (c) 25 μm, (d) 50 μm, (e) 100 μm and (f) 200 μm. The cross-sections of each speckle pattern at the maximum intensity from (g) to (l)

3.2. Speckle Patterns With Random Phases:

In realistic case, the mode propagation is effected by the obstackles like impurities or voids in the optical fiber and bending of fiber. As a result propagation of all modes change randomly. Therefore, the speckle at the output facet changes. We take these random variations by adding random phase to modes between 0 and 2π. We use the same parameters for as in Fig.3.1. The resulting output patterns are shown in Fig.3.2.

In 5-μm radius optical fiber intensity profile, the spot was shifted in y-direction and the spot size reduced to 3.23 μm. Moreover, the intensity of the core decreased. The intensity shifted to cladding of the optical fiber.

In 10-μm radius optical fiber intensity profile, there are new 2 spots formed and average spot size become 3.989 μm. Also, the intensity in the core decrease and shift to cladding.

In 25-um radius optical fiber, there are 4 spots with average size 6.532 μm. Also, the intensity in the core decreases and shift to cladding. In 50-μm radius optical fiber intensity profile, the average spot size becomes 6.477 μm.

It cannot be said the spot size increases with increasing fiber radius. The spot size only depends on the interference of the modes. Like previous patterns calculations in 3.1, as the V-number increases in the waveguide, we get more speckle patterns due to increase interfering of number of modes. By introducing different random phases, different speckles can be obtained. However, as the number of the modes decreases the fundamental LP_{01} mode dominates the output.

While random phases are added to all present modes in the waveguide, the speckle changes dramatically. The analysis of the correlation of the speckle patterns can provide means to develop fiber optic temperature sensors and mechanical sensors like extensometers.

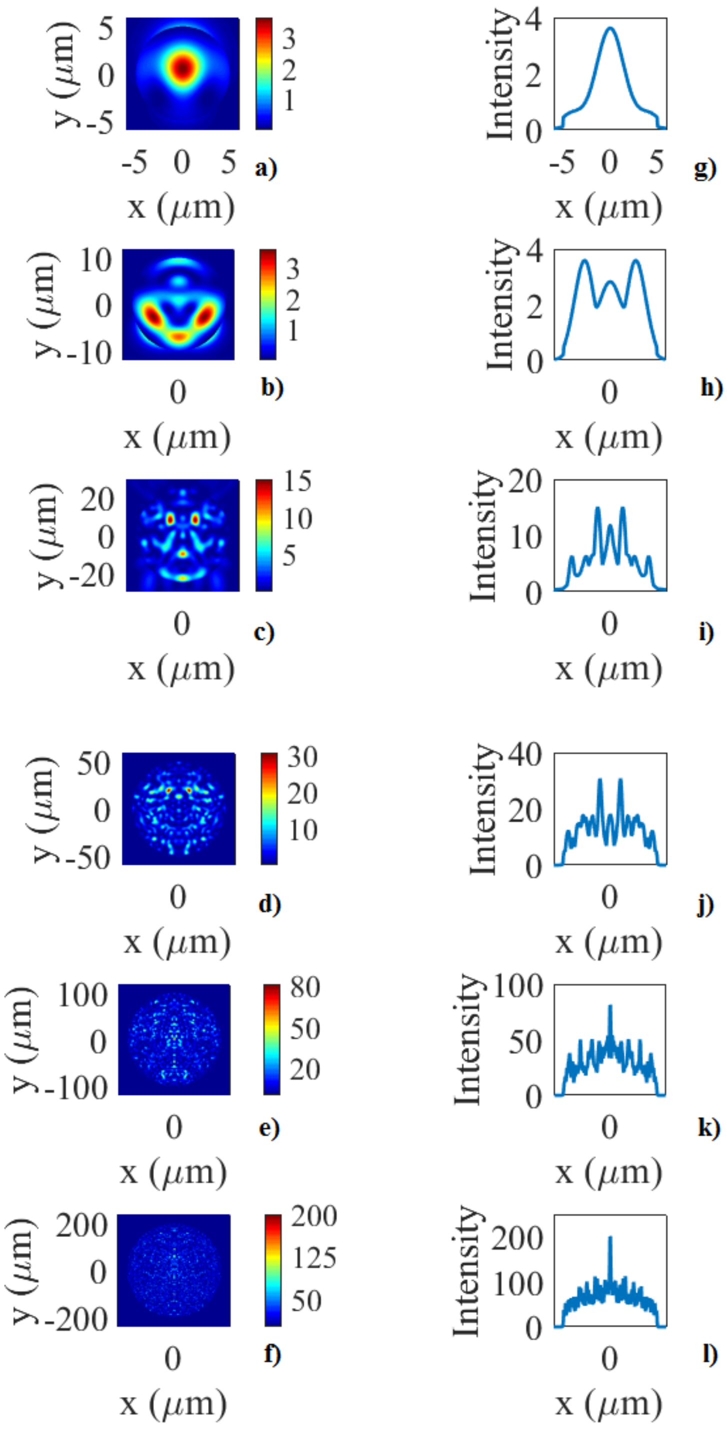

Figure 3.2. a) Calculated speckle pattern with random phases for a) 5 µm b) 10 µm. c) 25 µm d) 50 µm e) 100 µm f) 200 µm core radius size. The intensity profiles of highest peaks in the optical fibers of g) 5 µm h) 10 µm. i) 25 µm j) 50 µm k) 100 µm l

3.3. The Frequency Response of the Speckle Pattern:

Normalized frequency (the V-number) of the waveguide shows the wave propagation characteristics like the number of present modes and their propagation constants. As it seen from Eq.2.30, V-number also depends on the the wave number (therefore wavelength) of the coherent source propagating through optical fiber. When the wavelength of the light changes, both the number of the modes and their corresponding propagation constants change. Therefore, with combination of these two effects, the speckle at the output of the fiber also changes with changing input wavelength. In this section, we provide output intensity patterns at different input frequencies.

In imaging, correlation coefficient is used to find relationship and dependence between two different images. Correlation coefficient is used for observing the effect of frequency of light on speckle patterns. We use Pearson correlation coefficient which is calculated as[74]

$$r_{corr} = \frac{\sum_m \sum_n (A_{mn} - \overline{A})(B_{mn} - \overline{B})}{\sqrt{\sum_m \sum_n (A_{mn} - \overline{A})^2 \sum_m \sum_n (B_{mn} - \overline{B})^2}} \qquad \text{Eq.4.2.}$$

where A and B different matrices, $\bar{A}$ and $\overline{B}$ the mean values of all elements in A and B matrices.

In Fig.3.3., the correlation constants between speckle pattern obtained 1550 nm coherent source and other speckle patterns is shown within $\Delta\lambda = 4$ nm. From Fig.3.3., it can be said that as core radius and difference in the wavelength of the coherent source increases, the correlation decrease faster. While the correlation constant graphs both 25-50-100 um fibers shows a parabolic, there are some spikes in these plots. When the phase of some spatially large modes like low order modes is changed, there occurs a phase jump. This phase jump creates relatively large change in speckle pattern. As the phase change goes on with changing wavelength, the change in the speckle is reversed.

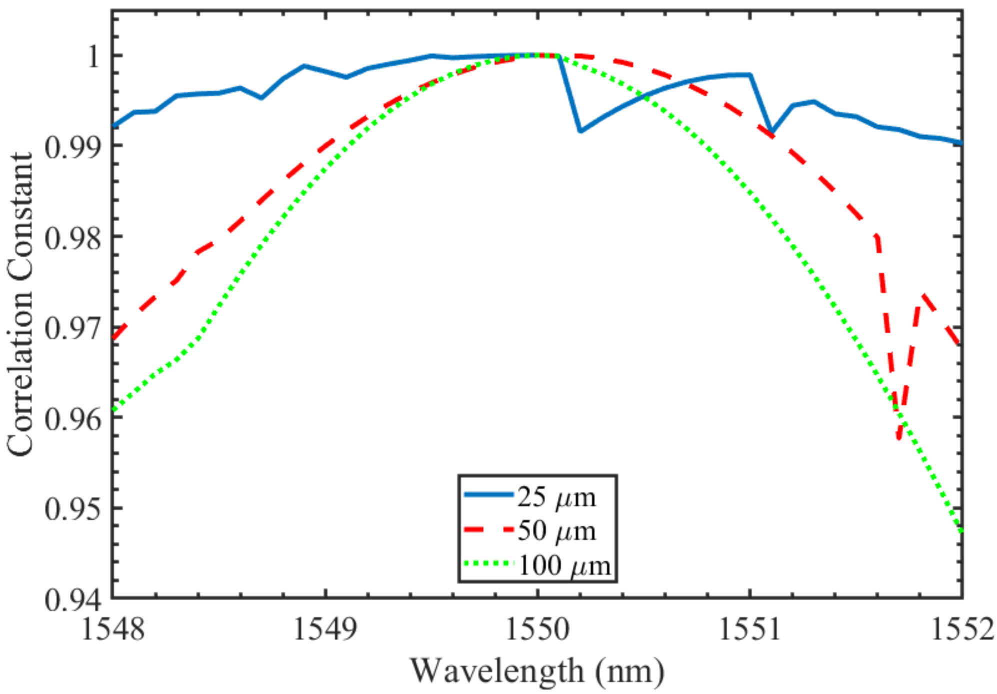

Figure 3.3. Transmitted intensity correlation of speckle pattern for 25 µm, 50 µm and 100 µm core radius fibers

In Fig.3.4, the calculated fiber outputs of 25-50-100-200 µm core radius fibers with 1550 and 1555 nm coherent sources are shown. Changing wavelength of the core makes dramatic changes in the speckle. For example, there are 3 new spots are formed in 25-µm core radius fiber by changing wavelength of the core. It can be said that wavelength of the light has great effect on speckle pattern. The correlation constants between 25 µm core radii fibers is 0.8286; between 50 µm core radii fibers is 0.6981; 100 µm core radii fibers is 0.4780 and 200 µm core radii fibers is 0.3306. Like Fig.3.3., as core radius increases, the correlation constants between speckle pattern decreases due to increased number of modes.

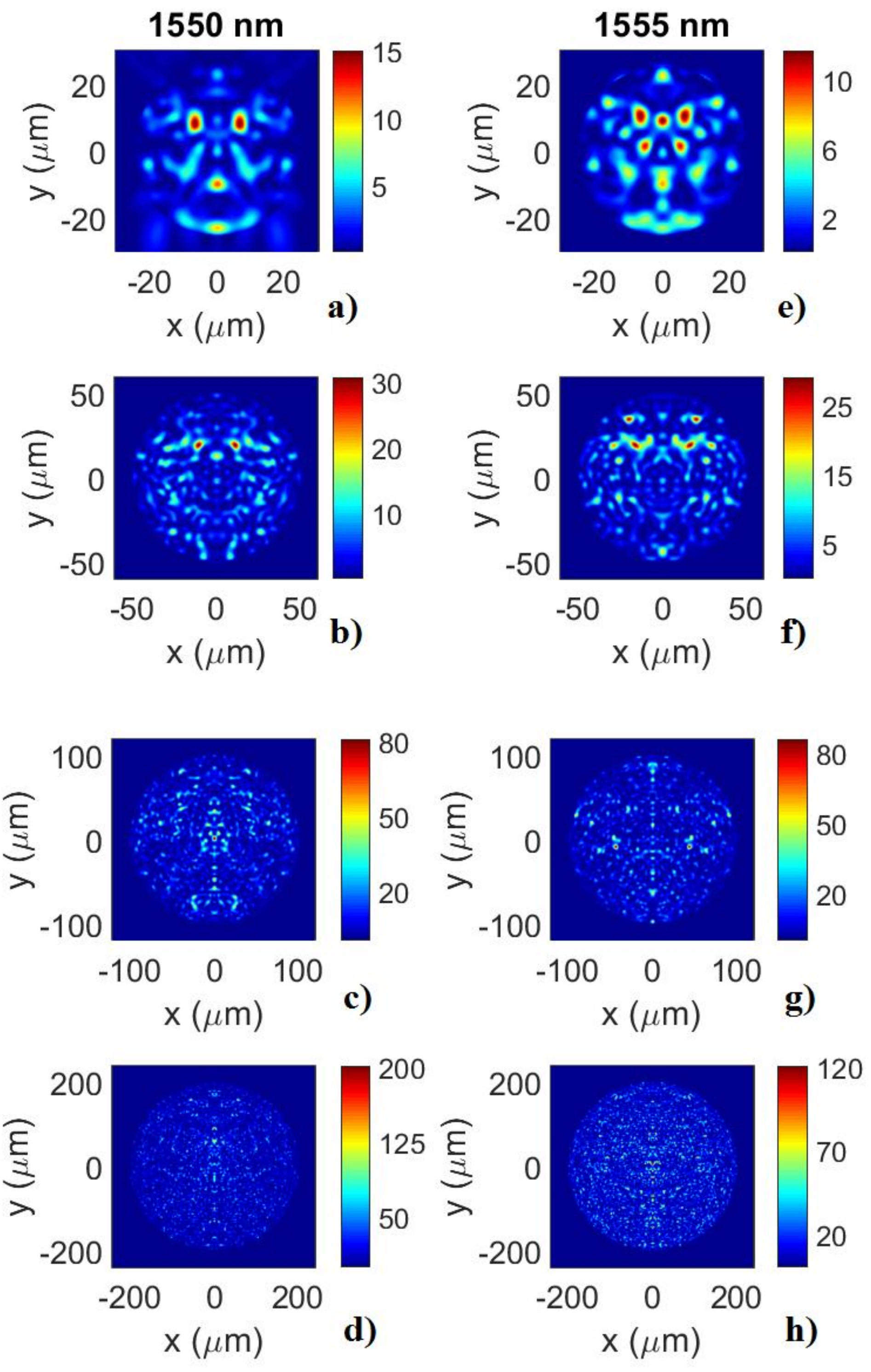

Figure 3.4. a-d) Calculated speckle patterns of 25-50-100-200 μm core radius fibers with 1550 nm coherent source, respectively. e-h) Calculated speckle patterns of 25-50-100-200 μm core radius fibers with 1555 nm coherent source, respectively.

3.4. Optimization of Speckle Patterns at the Output of Multimode Fibers:

The optimization is made by changing of phase of present modes in the optical fibers. In Fig.3.5., the superpositions of various wave fields (E_1, E_2, E_3, E_4) are shown. At the end, constructive interference is formed by changing the phase of the fields. Like in Fig.3.5., the phase change is made due to create total constructive or destructive interference at a specific area depending on optimization type. In our optimization process, the aim is to control interference of modes at the output of the fiber.

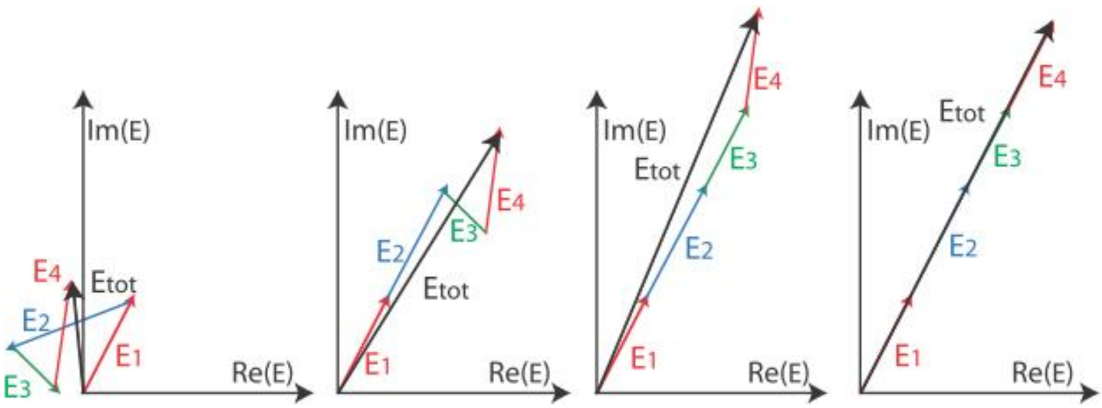

Figure 3.5. Representation of change in the phasor when optimization is done by changing phase of fields. The figure is adapted from [66-67].

Considering Eq.2.60., the change in the input field is replaced by adjusting new phases to the LP modes. The output of the fiber is changed by slipping the phases among modes.

3.4.1. Optimization to Increase Total Transmission:

We try to couple light to open transmission channels of fiber in order to increase the intensity of the optical fiber profile by introducing phases to the modes.

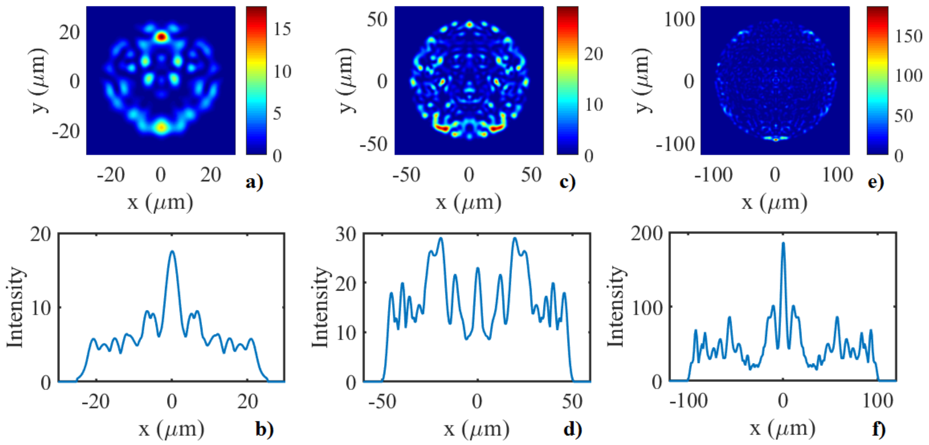

Figure 3.6. Calculated increasing optimized speckle pattern with random phases of a) 25 µm c) 50 µm e) 100 µm optical fibers and b-d-f) their intensity profiles, respectively.

In 25-µm radius optical fiber, the intensity distributed uniformly. However, several spots are observed in the speckle. The intensity in the core increases by 3.92%. In 50-µm radius optical fiber, the intensity is localized –y pole symmetrically. There are several spots formed –y pole. The intensity in the core increases by 6.29%. In 100-µm radius optical fiber, the intensity is distributed more uniformly. There is only one peak formed in the speckle in the –y pole. The intensity in the core increases by 0.77%.

From Fig.3.6., the speckles formed after optimization is uniform compared unoptimized speckles. Because the light is coupled to high transmission channel, the light has a ballistic transport.[72] This situation can be advantageous in medical applications specially in imaging and surgery. When the light is sent through open transmission channels, light can penetrate through tissue without scattering. Sending more light through fiber without any input power increase can ease the deep imaging through tissue.

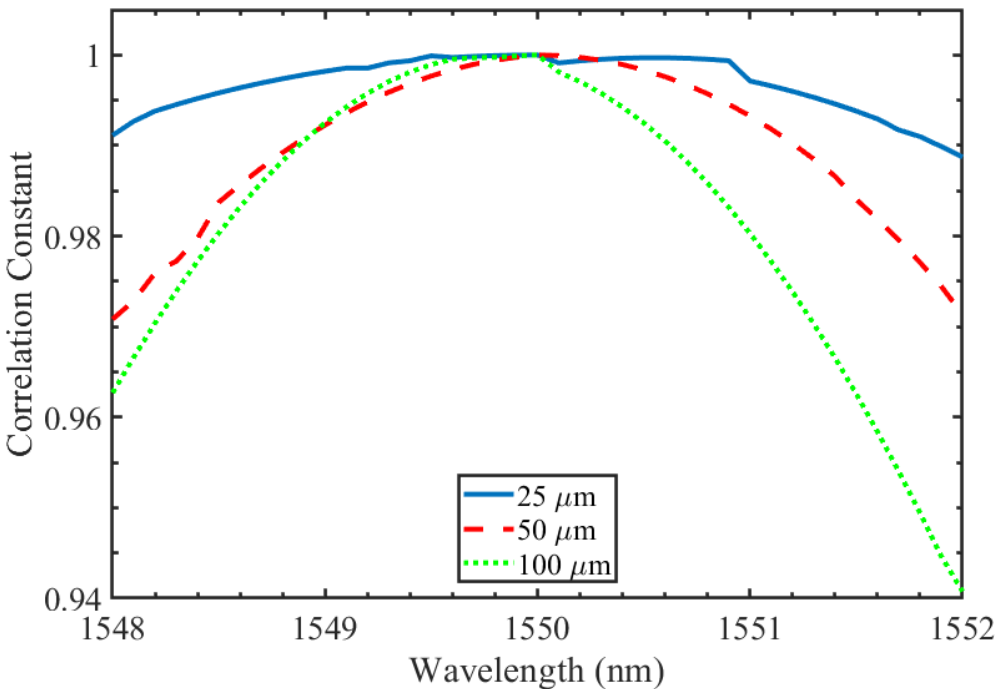

Figure 3.7. Transmitted intensity correlation of speckle pattern for 25 µm, 50 µm and 100 µm core radius fibers with increasing intensity at the output optimization

In Fig.3.7., it can be said that the speckle pattern at the output fiber changes dramatically both increasing core radius of the optical fiber and changing frequency of coherent source. Compared to Fig.3.4, optimization of intensity gives satisfactory results to change the speckle. The change in the speckle becomes more than the unoptimized case. In Fig.3.4., 100 µm core radius fibers the correlation constant between speckle patterns of 1548 nm and 1550 nm coherent sources is 0.96. In Fig.3.3., the correlation constants between speckle patterns of 1548 nm and 1550 nm coherent sources is 0.95.

3.4.2. Optimization of Light to a Single Spot

The optimization was made to increase intensity at one point in the core of optical fibers. There are three different optical fibers calculated and three different spots are calculated in these fibers.

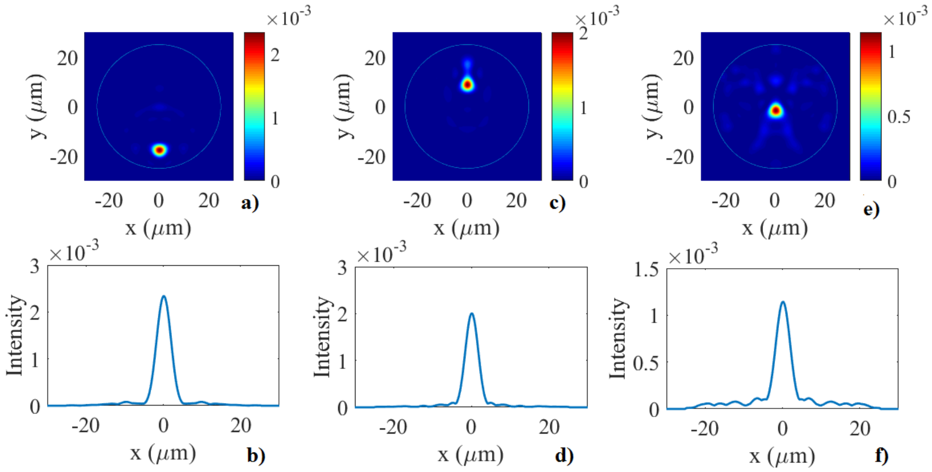

Figure 3.8. a) The intensity profile when the light is focused at x = 0, y = -20 µm b) its crossection at y = -20 µm c) focused at x = 0, y = 10 µm d) its crossection at y = 10 µm e) focused at x = 0, y = 0 µm d) its crossection at y = 0 µm

In Figure 3.8.a, the spot is at x = 0 & y = -20 µm of the fiber. The peak point at that point increases by nearly 40. FWHM of peak is 3.856 µm. In Figure 3.8.c, the spot is at x = 0 & y =10 µm. The peak point at that point increases by nearly 32. FWHM of peak is 4.478 µm. In Figure 3.8.e, the spot is in the center of the fiber. The peak point at that point increases by nearly 2. FWHM of peak is 6.36 µm.

Table 3.2. Intensity change after the optimization at different positions in 25 µm core radius optical fiber.

Position	Intensity Before Optimization	Intensity After Optimization	Change
y = 0 µm	$2*10^{-4}$	0.0011	550%
y = -20 µm	$2.08*10^{-4}$	0.00805	3870%
y = 10 µm	$1.12*10^{-4}$	0.00509	4550%

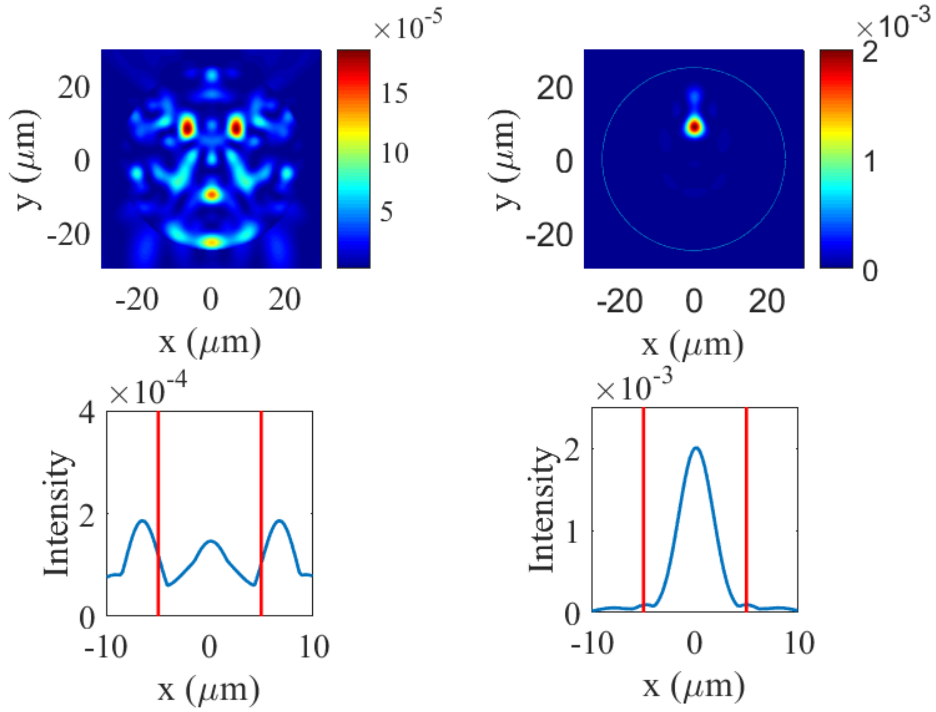

Figure 3.9. Calculated speckle patterns of 25 µm of optical fiber a) without any optimization b) its crossection at y = 10 µm c) one point optimization at x = 0 & y= 10 µm d) its crossection at y = 10 µm

In Fig.3.9., the intensity distributions of 25 µm core radius of optical fiber without any optimization and one point optimization of intensity at x = 0 & y = 10 µm are shown. After the optimization, the intensity distribution at one point increases nearly by a factor of 39. The calculation is made by integrating the areas of the intensity profiles. The other points' intensity change are shown in Table.3.2.

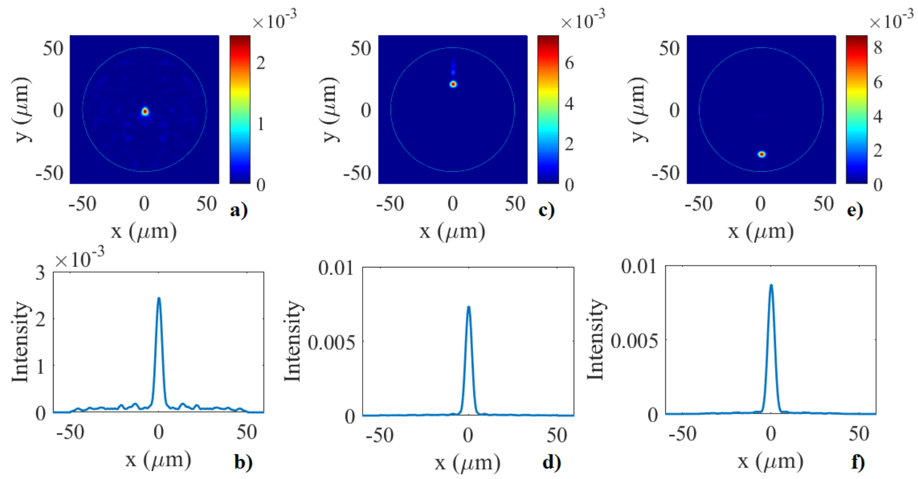

Figure 3.10. a) The intensity profile when the light is focused at x = 0, y = 0 µm b) its crossection at y = 0 µm c) focused at x = 0, y = 30 µm d) its crossection at y = 30 µm e) focused at x = 0, y = -40 µm d) its crossection at y = -40 µm

In Figure 3.10.a, the spot is in the center of the fiber. The peak point increases by nearly 1470 times. The FWHM of peak is 6.23 µm. In Figure 3.10.c, the spot is at x = 0 & y = 30 µm. The peak point increases by nearly 455 times. The FWHM of the peak is 4.189 µm. In Figure 3.10.e. the spot is at x = 0 & y =-40 µm. The peak point increases by nearly 1315 times. The FWHM of the peak is 6.23 µm.

Table 3.3. Intensity change after the optimization at different positions in 50 µm core radius optical fiber

Position	Intensity Before Optimization	Intensity After Optimization	Change
y = 0 µm	$3.70*10^{-4}$	0.01061	2870%
y = -40 µm	0.00100	0.0321	3200%
y = 30 µm	$3.70*10^{-4}$	0.04121	13900%

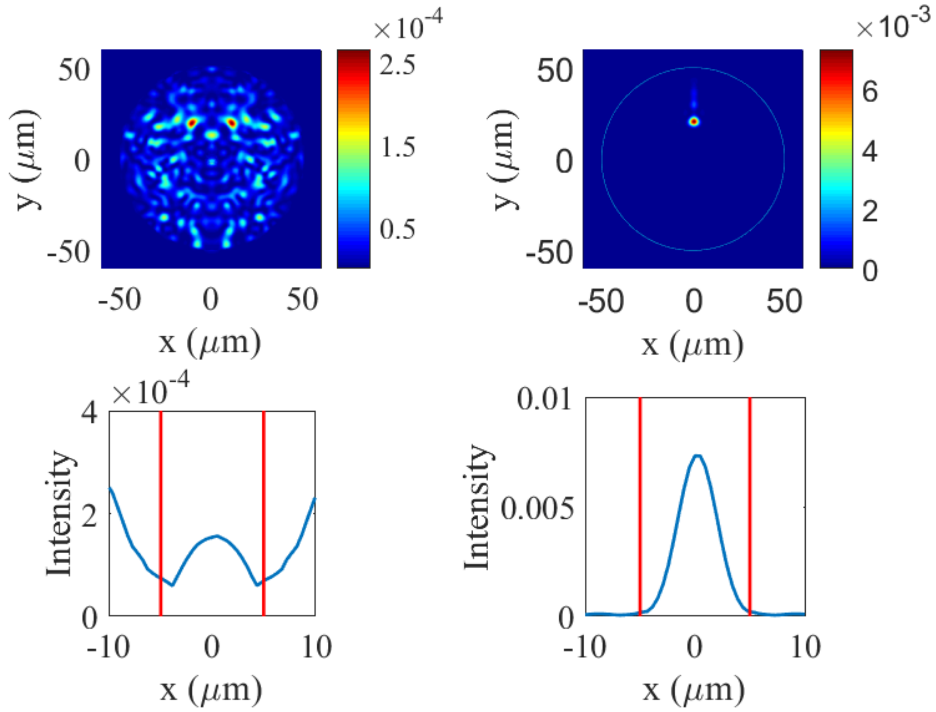

Figure 3.11. a) The intensity profile when the light is focused at x = 0, y = 0 µm b) its crossection at y = 0 µm c) focused at x = 0, y = 30 µm d) its crossection at y = 30 y = 30 µm e) focused at x = 0, y = -40 µm d) its crossection at y = -40 µm

In Fig.3.11., the intensity distributions of 50 µm core radius of optical fiber without any optimization and one point optimization of intensity at x = 0 & y = 30 µm are shown. After the optimization, the intensity distribution at one point increases nearly by a factor of 139 times. The other points' intensity change are shown in Table.3.3.

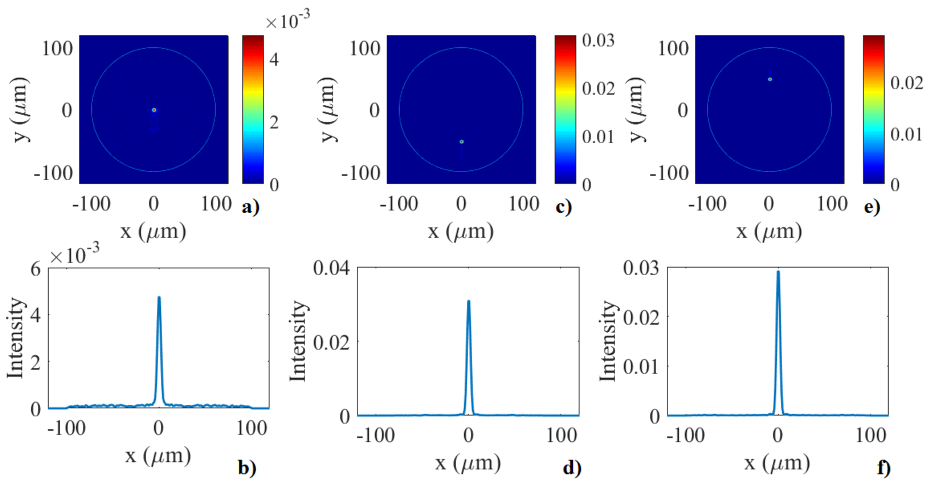

Figure 3.12. a) The intensity profile when the light is focused at x = 0, y = 0 µm b) its crossection at y = 0 µm c) focused at x = 0, y = -60 µm d) its crossection at y = -60 µm e) focused at x = 0, y = 60 µm d) its crossection at y = 60 µm

In Figure 3.12.a, the spot is in the center of the fiber. The peak point increases by nearly 23 times. The FWHM of the peak is 4.302 µm. In Figure 3.12.c, the spot is at x = 0 & y = -60 µm. The peak point increases by nearly 310 times. The FWHM of the peak is 4.40 µm. In Figure 3.12.e, the spot is at x = 0 & y = 60 µm. The peak point increases by nearly 6900 times. The FWHM of the peak is 4.261 µm.

Table 3.4. Intensity change after the optimization at different positions in 100 µm core radius optical fiber

Position	Intensity Before Optimization	Intensity After Optimization	Change
y = 0 µm	0.00106	0.02332	2200%
y = -60 µm	0.00118	0.13541	11450%
y = 60 µm	$3.70*10^{-5}$	0.04121	194500%

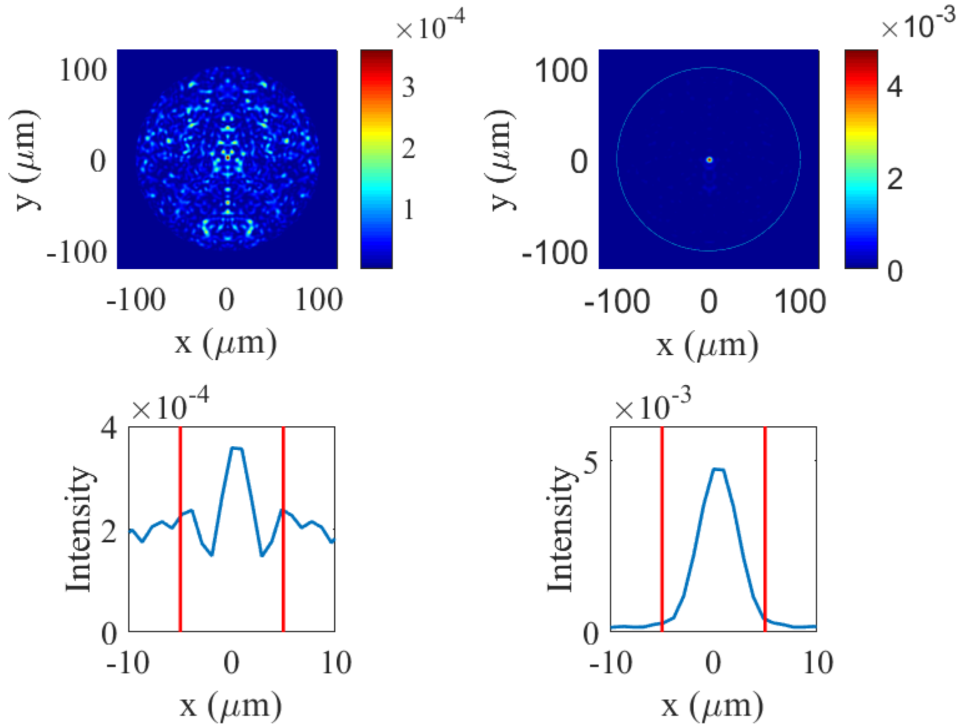

Figure 3.13. Calculated speckle patterns of 100 μm of optical fiber a) without any optimization b) its intensity profile at the center c) one point optimization at the center and d) its crossection at the center

In Fig. 3.13., the intensity distributions of 100 μm core radius of optical fiber without any optimization and one point optimization of intensity at the center are shown. After the optimization, the intensity distribution at one point increases nearly by a factor of 22. Other points' intensity change are shown in Table.3.4.

It can be said that as the number of the modes present in the fiber increases, the intensity of optimized light on one point increses. This is due to increase in the mode number. Many modes can be modulated on a specific point. Moreover, the optimized intensity of the light at +y and –y hemi-circles is more than those of at the center. The intensity change at one point is up to thousand times. This huge intensity change enables modulation of light through fiber for information technologies.

3.4.3. Speckle Patterns at Output of the Fiber with Decreasing Optimization:

In order to decrease the transmission of light through optical fiber, the open transmission channels of light should be blocked by destructive interference while propagation. The optimization was made to decrease the intensity of core of the optical fiber profile by adding phases to the modes by creating destructive interference among modes.

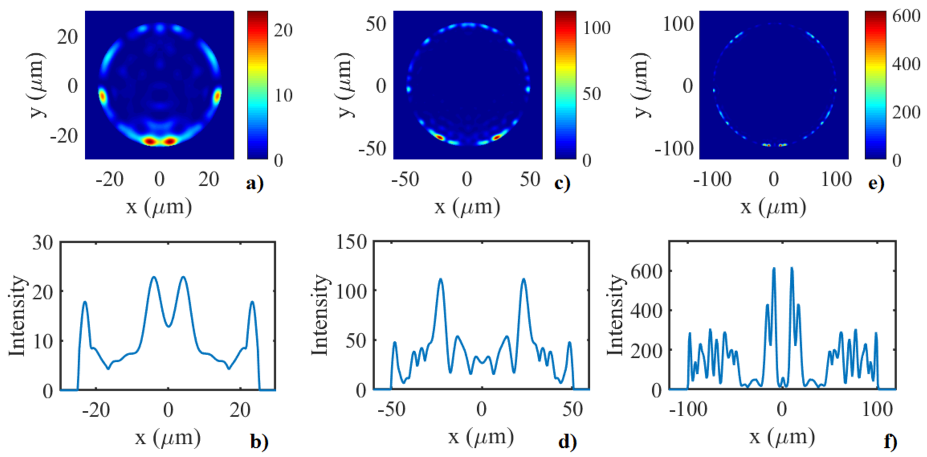

Figure 3.14. a) Calculated decreasing optimized speckle pattern with random phases of a) 25 µm c) 50 µm e) 100 µm. The crossections of each panel is provided on the lower panels for b) 25 µm d) 50 µm f) 100 µm fiber radius

In 25-µm radius optical fiber, the intensity shifts to the near the core-cladding interface. There are 4 peaks forms at the core-cladding interface. These peaks have an average spot size 4,081 µm. The intensity in the core drops by 21.4%.

In 50-µm radius optical fiber, the intensity shifts to the near the core-cladding interface. There are 4 peaks forms at the core-cladding interface. These peaks have an average spot size 5.987 µm. The intensity in the core drops by 2.75%.

In 100-µm radius optical fiber, the intensity shifts to the near the core-cladding interface. There are 13 peaks forms at the core-cladding interface. The intensity in the core drops by 8.55%.

The speckle in the decreasing optimized optical fiber is localized around core-cladding interface. This is expected since optical path length of the modes are increased. At interfaces, the intensity is not continuous, several spots are formed. Intensity decreasing optimization can be used for grouping specific modes in the waveguides. Chosen modes can be placed in the center of the optical fibers and remaining modes are shifted to the core-cladding interface or annihilated creating destructive interference among the modes.

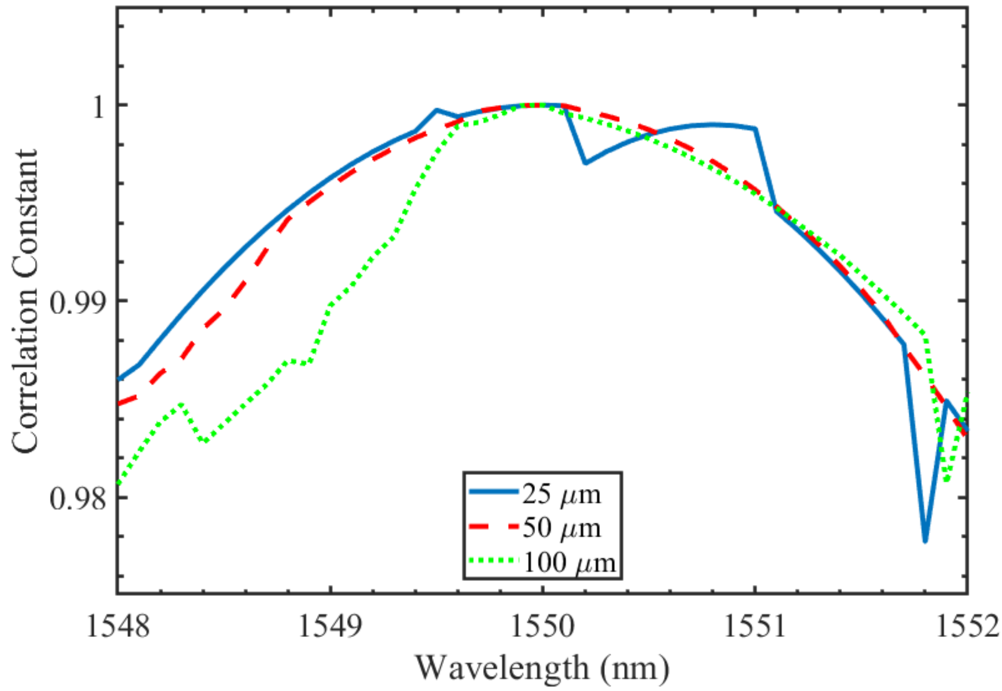

Figure 3.15. Transmitted intensity correlation of speckle pattern for 25 μm, 50 μm and 100 μm core radius fibers with decreasing intensity at the output optimization

In Fig.3.15., it can be said that the speckle pattern at the output fiber changes dramatically both increasing core radius of the optical fiber and changing frequency of coherent source. Although, the change in the correlation constants shows a parabolic behavior, there are some spikes in the graphs. Compared to Fig.3.3. and Fig.3.7., the change in the speckle in decreasing intensity optimization with decreasing wavelength is slower those of increasing intensity optimization since speckle pattern at the output of the fiber is lost. Intensity distribution is at mostly core-cladding interface.

3.5. Spatial Mode Division and Multiplexing:

LP_{01} mode is the fundamental mode which has the highest propagation constant in the fiber. This makes it dominant in the speckle. In previous optimizations, all modes are optimized to obtain desired patterns. For example, in one point optimization, phases are assigned to modes in order to create one focus in the optical fiber.

In this section, we try to show intensity change of the center of the core of optical fiber by changing the phase of one and two modes together. The effect of changing the phase of one or two modes in the waveguides is explained. Firstly, the effect of LP_{01} mode on speckle is inspected. Then, both LP_{01} and LP_{35} modes on speckle is inspected. Their correlation calculations of optimized and unoptimized speckles are compared.

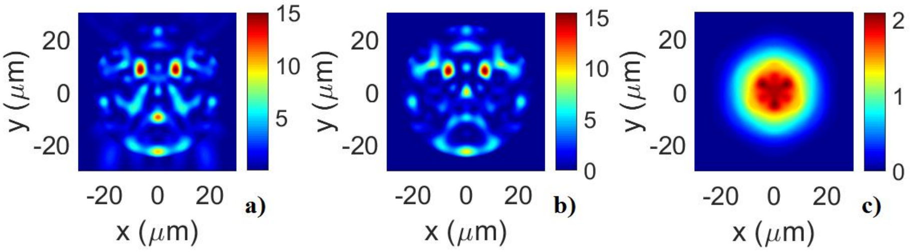

Figure 3.16. a). The resultant speckle of 25 μm optical fiber without any phase addition. b). The resultant speckle of 25 μm optical fiber with phase added to LP_{01} mode c). The difference in the speckle when the phase added to LP_{01}

In Fig.3.16., the maximum intensity change in the center of the fiber is obtained when $3\pi/2$ phase added to LP_{01} mode. There are several changes in the speckle pattern. The intensity distribution has shifted to +y hemi-circle. The intensity increase in the center of the fiber is 80%. The correlation constant between optimized and unoptimized speckles is 0.82.

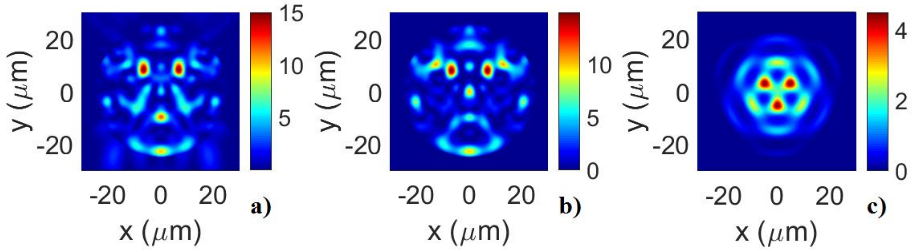

Figure 3.17. a). The resultant speckle of 25 μm optical fiber without any phase addition. b). The resultant speckle of 25 μm optical fiber with phase added to LP_{01} and LP_{35} modes c). The difference in the speckle when the phase added to LP_{01} and LP_{35} modes

From Fig. 3.17., when the phase $3\pi/2$ added to LP_{01} and $11\pi/8$ LP_{35} modes, the hightest change in the center of the core is obtained. However, the spots formed at the +y hemi-circle have lower intensity than the unoptimized speckle. The intensity increase at the center of the optical fiber is around 81%. The correlation constants of optimized and unoptimized speckles is 0.72.

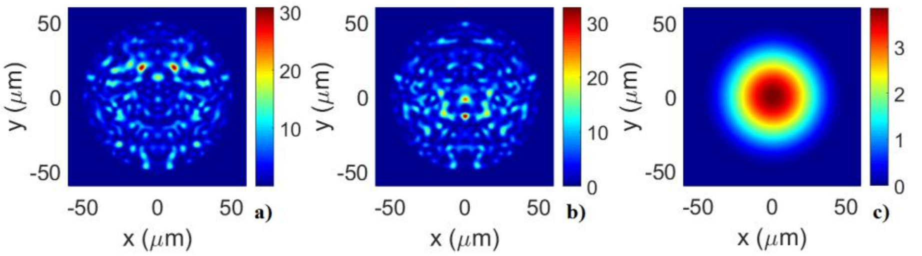

Figure 3.18. a). The resultant speckle of 50 μm optical fiber without any phase addition. b). The resultant speckle of 50 μm optical fiber with phase added to LP_{01} mode c). The difference in the speckle when the phase added to LP_{01}

It is seemed from Fig. 3.18., when the phase $9\pi/8$ added to LP_{01}, the two spots at the y hemi-circle diminish and the intensity of spot at –y hemi-circle has increased. The intensity at the center is doubled. The correlation constants of optimized and unoptimized speckles is 0.745.

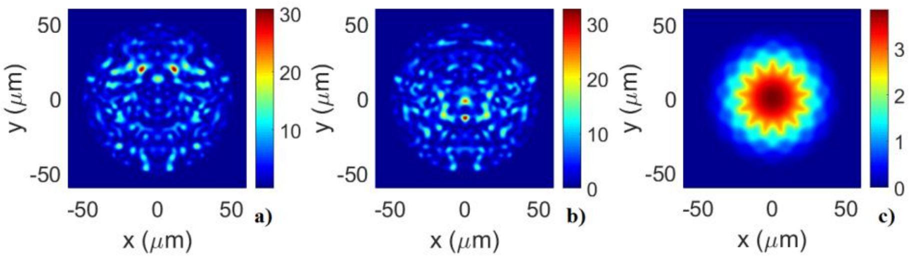

Figure 3.19. a). The resultant speckle of 50 μm optical fiber without any phase addition. b). The resultant speckle of 50 μm optical fiber with phase added to LP_{01}

and LP_{35} modes c). The difference in the speckle wheen the phase added to LP_{01} and LP_{35}

When $9\pi/8$ phase added to LP_{01} and $7\pi/4$ phase added to LP_{35}, the previous speckle changes occurs when the phase of LP_{35} mode is changed. The change in the intensity at the center of the core is nearly same. The correlation constants of optimized and unoptimized speckles is 0.735. The results are satisfactory like one point optimization case.

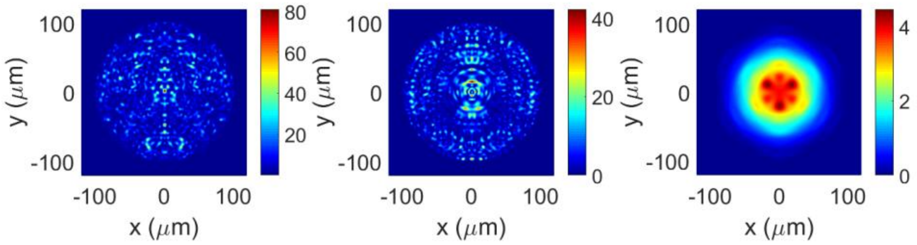

Figure 3.20. The resultant speckle of 100 μm optical fiber when phase added to LP_{01} mode. b). The resultant speckle of 100 μm optical fiber without any optimization c). The resultant speckle of 100 μm optical fiber when π phase added to LP_{01} mode

When the phase $9\pi/8$ added to LP_{01} mode, the spots at the center diminish and new 4 spots are formed at the +y hemi-circle. The intensity at the center of the fiber is increased by 30%. The correlation constants of optimized and unoptimized speckles is 0.82.

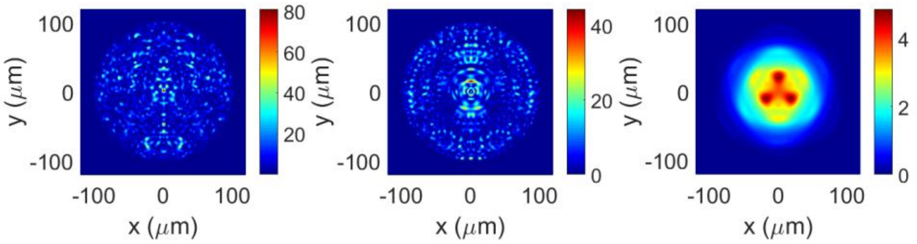

Figure 3.21. a). The resultant speckle of 100 μm optical fiber without any phase addition. b). The resultant speckle of 100 μm optical fiber with phase added to LP_{01} and LP_{35} modes c). The difference in the speckle wheen the phase added to LP_{01} and LP_{35} modes

When 9π/8 phase is added to both LP_{01} and 7π/4 phase is added to LP_{35}, the intensity change is around 30%. The correlation constants of optimized and unoptimized speckles is 0.805.

In study of Carpenter et al[55], they programmed phase masks on the surface of SLM in order to demultiplex of all modes and change the phase of modes individually.

Table 3.5. The intensity change and correlation constants between optimized and unoptimized speckle patterns obtained at the output different optical fibers

Fiber Core Radius	Intensity Change (LP_{01})	Correlation Constants (LP_{01})	Intensity Change (LP_{01}&LP_{35})	Correlation Constants (LP_{01}&LP_{35})
25 μm	80%	0.82	80%	0.72
50 μm	100%	0.745	100%	0.735
100 μm	30%	0.82	30%	0.805

Although the intensity change is not much as optimizing light to one spot, the intensity change at the center of the fiber gives satisfactory results by changing phase of LP_{01}. In 50 µm core radius fiber, the intensity change is doubled. However, the high order LP_{35} mode nearly has no effect the intensity change. The modulation of high order mode has effect on the speckle pattern. Shifting the relative phase LP_{35} decreases correlation between speckles.

As the number of the supported modes increases in the optical fiber, correlation constants approaches to 1. The effect of the LP_{01} mode decreases dramatically when the number of the modes increases. Both calculating correlation constants and intensity changes at a specific points gives satisfactory results for optical modulation. Intensity changes at specific points depends on the interference among modes. If the interference change after changing modes of the phases is mapped, we can find where most drastic change of intensity.

CHAPTER IV

CONCLUSIONS

In this thesis, a method is developed to optimize speckle pattern at the output of a multimode fiber by controlling interference at output of the fiber. Before the intensity optimization, speckle patterns of various optical fibers has been calculated. Also, in order to observe the effect of perturbations like bending or voids in optical fibers, additional calculations has been made by introducing random phases to modes. In order to observe the effect of wavelength of light on speckle pattern, speckle patterns of various optical fibers were calculated within $\Delta\lambda = 4$ nm.

First optimization is increasing the total transmission at the output of the fiber. In this optimization, light is sent through the high transmission channels by controlling interference among modes introducing new phases between 0 and 2π. The output of three different optical waveguide was optimized. In 25 µm core radius optical fiber, the intensity at the output of fiber increased by 3.92%. In 50 µm core radius optical fiber, the intensity at the output of fiber increased by 6.29%. In 100 µm core radius optical fiber, the intensity at the output of fiber increased by 0.77%. Also, the speckle changes faster than unoptimized case with changing wavelength of light.

Secondly, the light was optimized to create a single spot at the output of the fiber. Again, there was optimized three different optical fibers and there are three different spots formed in each waveguide separately. In 100 µm core optical fiber, the intensity increased by 1945 times at the optimized point.

Then, the light was optimized to decrease the total transmission of the fiber by creating destructive interference at the output. This was made by blocking the transmission channels through the fiber. In 25 µm core radius optical fiber, the intensity at the output of fiber decreased by 21.4%. In 50 µm core radius optical fiber, the intensity at the output of fiber decreased by 2.75%. In 100 μm core radius optical fiber, the intensity at the output of fiber decreased by 8.55%. In resultant speckles for all optical fibers, the intensity was shifted to core-cladding interface due to increase in the optical path length during optimization. Like in increasing the total transmission, the speckle changes faster than unoptimized case with changing wavelength of the light.

Finally, the intensity change at the center of the fiber and the speckle change of the core of optical fiber was inspected by modulating one (LP_{01}) and two modes (LP_{01} and LP_{35}) together. The intensity was doubled at the center of fiber by modulating only LP_{01} mode in 50 μm core optical fiber. Although the intensity change is not high as optimizing to create one spot, this intensity change is sufficient to create optical modulator.

The results found in this thesis study can be used in communication and biomedical technologies. By optimizing light to a single spot, intensity change at one point is so huge that this intensity change enables modulation of light through fiber for information technologies. Moreover, increasing the total transmission through fiber can be advantageous for biophotonics and medical applications, especially deep imaging through tissue.

In this thesis, we did not consider the effect of noise and mode coupling. If these effects can be added to calculations, more realistic results can be obtained. In our optical fiber model, it is assumed that refractive index distribution is isotropic for both core and cladding. Therefore, effective index method is not considered in the calculations.

REFERENCES

1. Sheng, P. (2011). Introduction to wave scattering, localization and mesoscopic phenomena. Berlin: Springer.

2. Wiersma, D., Colocci, M., Righini, R., & Aliev, F. (2001). Temperature-controlled light diffusion in random media. Physical Review B, 64(14)

3. Zhu, J. X., Pine, D. J., & Weitz, D. A. (1991). Internal reflection of diffusive light in random media. Physical Review A, 44(6), 3948-3959.

4. Akkermans, E., & Montambaux, G. (2011). Mesoscopic physics of electrons and photons. Cambridge: Cambridge Univ Press.

5. Imry, Y. (2009). Introduction to mesoscopic physics. Oxford: Oxford University Press.

6. Ishimaru, A. (2005). Wave propagation and scattering in random media. Piscataway, NJ: IEEE Press.

7. Roach, G. F. (2009). Wave Scattering by Time-Dependent Perturbations An Introduction. Princeton: Princeton University Press.

8. Murayama, Y. (2001). Mesoscopic systems: fundamentals and applications. Weinheim: Wiley-VCH.

9. Lagendijk, A., & Tiggelen, B. A. (1996). Resonant multiple scattering of light. Physics Reports, 270(3), 143-215.

10. Hulst, H. C. (2009). Light scattering by small particles. New York, NY: Dover.

11. Ferry, D. K., Goodnick, S. M., & Bird, J. P. (2011). Transport in nanostructures. Cambridge: Cambridge University Press.

12. Datta, Supriyo (2009). Electronic transport in mesoscopic systems. Cambridge: Cambridge Univ. Press.

13. Mello, Pier A., and N. Kumar (2010). Quantum transport in mesoscopic systems: complexity and statistical fluctuations: a maximum entropy viewpoint. Oxford: Oxford University Press.

14. Beenakker, C. W. J. (1997). "Random-matrix theory of quantum transport." Reviews of Modern Physics 69, no. 3.

15. Pichard, J.-L. (2001). "Random Matrix Theory of Scattering in Chaotic and Disordered Media." Waves and Imaging through Complex Media.

16. Rotter, Stefan, and Sylvain Gigan (2017). "Light fields in complex media: Mesoscopic scattering meets wave control." Reviews of Modern Physics 89, no. 1.

17. Beckers, J. M. (1992). Adaptive Optics For Astronomy: Principles, Performance And Applications : Eso Scientific Preprint No.877. [S.l.]: European Southern Observatories.

18. M. Vellekoop and A. P. Mosk, (2007). "Focusing coherent light through opaque strongly scattering media," Opt. Lett. 32, 2309-2311.

19. Vellekoop, I. M., A. Lagendijk, and A. P. Mosk, (2010). Exploiting disorder for perfect focusing. Nature Photonics.

20. Donald B. Conkey and Rafael Piestun, (2012). "Color image projection through a strongly scattering wall," Opt. Express 20, 27312-27318

21. Vellekoop, I. M., and A. P. Mosk, (2008). "Universal Optimal Transmission of Light Through Disordered Materials." Physical Review Letters 101, no. 12

22. Kim, M., Choi, Y., Yoon, C., Choi, W., Kim, J., Park, Q. H., & Choi, W. (2012). Maximal energy transport through disordered media with the implementation of transmission eigenchannels. Nature Photonics, 6(9), 581-585

23. J. H. Park, C. H. Park, H. Yu, Y. H. Cho, and Y. K. Park, (2012). Active spectral filtering through turbid media, Opt. Lett. 37, 3261-3263.

24. J.-H. Park, C. Park, H. Yu, Y.-H. Cho, and Y. Park, (2012). Dynamic active wave plate using random nanoparticles, Opt. Exp. 20, 17010-17016.

25. Santosh Tripathi, Richard Paxman, Thomas Bifano, and Kimani C. Toussaint, (2012). Vector transmission matrix for the polarization behavior of light propagation in highly scattering media, Opt. Express 20, 16067-16076

26. Santosh Tripathi and Kimani C. Toussaint, (2014). Harnessing randomness to control the polarization of light transmitted through highly scattering media, Opt. Express 22, 4412-4422.

27. J. Aulbach, B. Gjonaj, P. M. Johnson, A. P. Mosk, and A. Lagendijk, (2011). Control of light transmission through opaque scattering media in space and time, Physical Review Letters 106, 103901.

28. K. Lee, J. Lee, J. H. Park, J. H. Park, and Y. Park, (2015). "One-Wave Optical Phase Conjugation Mirror by Actively Coupling Arbitrary Light Fields into a Single Mode Reflector," Phys Rev Lett 115.

29. Jonathan V. Thompson, Brett H. Hokr, Vladislav V. Yakovlev, (2017). "Improved light injection and enhanced Raman scattering in microfabricated opaque structures," Proc. SPIE 10112, Photonic and Phononic Properties of Engineered Nanostructures VII, 101120S.

30. O. Katz, E. Small, Y. Guan, and Y. Silberberg, (2014). "Noninvasive nonlinear focusing and imaging through strongly scattering turbid layers," Optica 1, 170-174.

31. Hadas Frostig, Eran Small, Anat Daniel, Patric Oulevey, Stanislav Derevyanko, and Yaron Silberberg, (2017). "Focusing light by wavefront shaping through disorder and nonlinearity," Optica 4, 1073-1079.

32. Tomáš Čižmár and Kishan Dholakia, (2009). "Tunable Bessel light modes: engineering the axial propagation," Opt. Express 17, 15558-15570.

33. Ambichl, P., Brandstötter, A., Böhm, J., Kühmayer, M., Kuhl, U. and Rotter, S.. (2017). Focusing inside Disordered Media with the Generalized Wigner-Smith Operator. Physical Review Letters, 119(3).

34. R. Horstmeyer, H. W. Ruan, and C. H. Yang, (2015). "Guidestar-assisted wavefront-shaping methods for focusing light into biological tissue," Nature Photonics 9, 563-571.

35. Vellekoop, I. M., and C. M. Aegerter. (2010). "Focusing light through living tissue." Optical Coherence Tomography and Coherence Domain Optical Methods in Biomedicine XIV.

36. H. Yu, J. Jang, J. Lim, J. H. Park, W. Jang, J. Y. Kim, and Y. Park, (2014). "Depth-enhanced 2-D optical coherence tomography using complex wavefront shaping," Optics Express 22, 7514-7523.

37. J. Yoon, M. Lee, K. Lee, N. Kim, J. M. Kim, J. Park, C. Choi, W. D. Heo, and Y. Park, (2015). "Optogenetic control of cell signaling pathway through scattering skull using wavefront shaping," Sci Rep 5, 13289.

38. Liew, S. F., Popoff, S. M., Sheehan, S. W., Goetschy, A., Schmuttenmaer, C. A., Stone, A. D., & Cao, H. (2016). Coherent Control of Photocurrent in a Strongly Scattering Photoelectrochemical System. ACS Photonics, 3(3), 449-455.

39. J. Park, J.-Y. Cho, C. Park, K. Lee, H. Lee, Y.-H. Cho, and Y. Park, (2016). "Scattering Optical Elements: Stand-Alone Optical Elements Exploiting Multiple Light Scattering," ACS Nano.

40. H. Yu, K. Lee, J. Park, and Y. Park, (2017). "Ultrahigh-definition dynamic 3D holographic display by active control of volume speckle fields," Nature Photonics.

41. Paivasaari, K., Silvennoinen M., Kaakkunen J., Vahimaa P., "Femtosecond laser processing and spatial light modulator," (2014). Proc. SPIE 8967, Laser Applications in Microelectronic and Optoelectronic Manufacturing (LAMOM) XIX, 89670F.

42. Liutkus, A., Martina, D., Popoff, S., Chardon, G., Katz, O., Lerosey, G., .Carron, I. (2014). Imaging With Nature: Compressive Imaging Using a Multiply Scattering Medium. Scientific Reports, 4(1).

43. Goorden, S. A., Horstmann, M., Mosk, A. P., Škorić, B., & Pinkse, P. W. (2014). Quantum-secure authentication of a physical unclonable key. Optica, 1(6), 421.

44. Jump to Fiber Optics Training Provider. (n.d.). Retrieved November 28, 2017, from https://arcelect.com/fibercable.htm

45. Cizmar, T. and Dholakia K., (2012). "Exploiting multimode waveguides for pure fibre-based imaging," Nat Commun 3.

46. Papadopoulos, I. N., Farahi, S., Moser, C. , and Psaltis, D., (2013). "Increasing the imaging capabilities of multimode fibers by exploiting the properties of highly scattering media," Opt. Lett. 38, 2776-2778.

47. Mahalati R. N., Yu Gu R., and Kahn J. M., (2013). "Resolution limits for imaging through multi-mode fiber," Opt. Express 21, 1656-1668.

48. Plöschner, M., Tyc, T., & Čižmár, T. (2015). Seeing through chaos in multimode fibres. Nature Photonics, 9(8), 529-535

49. Čižmár, T., & Dholakia, K. (2011). Shaping the light transmission through a multimode optical fibre: complex transformation analysis and applications in biophotonics. Optics Express, 19(20), 18871.

50. Liew, S. F., Redding, B., Choma, M. A., Tagare, H. D., & Cao, H. (2016). Broadband multimode fiber spectrometer. 2016 IEEE Photonics Society Summer Topical Meeting Series (SUM).

51. Choi, Y., Yoon, C., Kim, M., Yang, T. D., Fang-Yen, C., Dasari, R. R., . . . Choi, W. (2012). Scanner-Free and Wide-Field Endoscopic Imaging by Using a Single Multimode Optical Fiber. Physical Review Letters, 109(20).

52. Papadopoulos, I. N., Farahi, S., Moser, C., & Psaltis, D. (2013). High-resolution, lensless endoscope based on digital scanning through a multimode optical fiber. Biomedical Optics Express, 4(2), 260.

53. Popoff, S., Lerosey, G., Fink, M., Boccara, A. C., & Gigan, S. (2010). Image transmission through an opaque material. Nature Communications, 1(6), 1-5.

54. Delrot, P., Loterie, D., Psaltis, D., & Moser, C. (2018). Single-photon three-dimensional microfabrication through a multimode optical fiber. Optics Express, 26(2), 1766.

55. Carpenter, J. , Thomsen, B. C. and Wilkinson, T. D., (2012). "Degenerate Mode-Group Division Multiplexing," J. Lightwave Technol. 30, 3946-3952.

56. Xiong, W., Ambichl, P., Bromberg, Y., Redding, B., Rotter, S., & Cao, H. Principal modes of a multimode fiber with strong mode coupling. 2016 IEEE Photonics Society Summer Topical Meeting Series (SUM).

57. Xiong, W., Ambichl, P., Bromberg, Y., Redding, B., Rotter, S. and Cao, H. (2016). Spatiotemporal Control of Light Transmission through a Multimode Fiber with Strong Mode Coupling. Physical Review Letters, 117(5).

58. Ambichl, P., Xiong, W., Bromberg, Y., Redding, B., Cao, H. and Rotter, S. (2017). Super- and Anti-Principal-Modes in Multimode Waveguides. *Physical Review X*, 7(4).

59. Popoff, S. M., G. Lerosey, R. Carminati, M. Fink, A. C. Boccara, and S. Gigan. (2010). "Measuring the Transmission Matrix in Optics: An Approach to the Study and Control of Light Propagation in Disordered Media." Physical Review Letters 104, no. 10

60. Bianchi, S., and Di Leonardo, R., (2012). "A multi-mode fiber probe for holographic micromanipulation and microscopy." Lab Chip 12, no.3 : 635-39.

61. Papadopoulos, I. N., Farahi, S., Moser, C., & Psaltis, D. (2013). High-resolution, lensless endoscope based on digital scanning through a multimode optical fiber. Biomedical Optics Express, *4*(2), 260–270.

62. T. Okamoto and I. Yamaguchi, (1988) . “Multimode fiber-optic Mach-Zehnder interferometer and its use in temperature measurement,” Appl. Opt. 27(15), 3085–3087

63. K. Pan, C. M. Uang, F. Cheng, and F. T. Yu, (1994). “Multimode fiber sensing by using mean-absolute speckle-intensity variation,” Appl. Opt. 33(10), 2095–2098.

64. Oraby, O. A., Spencer, J. W., and Jones, G. R., (2009). “Monitoring changes in the speckle field from an optical fibre exposed to low frequency acoustical vibrations,” J. Mod. Opt. 56(1), 55–84.

65. Fujiwara, E. , Wu, Y. T., and Suzuki, C. K., (2012). “Vibration-based specklegram fiber sensor for measurement of properties of liquids,” Opt. Lasers Eng. 50(12), 1726–1730.

66. Redding, B. and Cao, H., (2012). "Using a multimode fiber as a high-resolution, low-loss spectrometer," Opt. Lett. 37, 3384-3386.

67. Redding, B., Popoff, S. M. and Cao, H., (2013). "All-fiber spectrometer based on speckle pattern reconstruction," Opt. Express 21, 6584-6600.

68. Chen, K., Zhang, J., Nong, Z., Cai, X., He, S., & Liu, L. (2017). Compact Multimode 3dB Coupler for On-chip Mode Division Multiplexing. Optical Fiber Communication Conference

69. Tsekrekos, C. P., and Syvridis, D., (2012). "All-Fiber Broadband LP_{02} Mode Converter for Future Wavelength and Mode Division Multiplexing Systems." IEEE Photonics Technology Letters 24, no. 18

70. "Research at CMMPE - Devices & applications - Liquid crystals for telecommunications." CMMPE - University of Cambridge. Accessed January 25, 2018. http://www-g.eng.cam.ac.uk/CMMPE/telecoms.html.

71. Snitzer, E., (1961). "Cylindrical Dielectric Waveguide Modes*," J. Opt. Soc. Am. 51, 491-498.

72. Gloge, D. (1971). "Weakly Guiding Fibers." Applied Optics 10, no. 10 228 - 239.

73. Descloux, A., Amitonova, L. V., & Pinkse, P. W. (2016). Aberrations of the point spread function of a multimode fiber due to partial mode excitation. Optics Express, 24(16), 18501. doi:10.1364/oe.24.018501

74. Corrcoef. (n.d.). Retrieved January 20, 2018, from https://www.mathworks.com/help/images/ref/corr2.html

75. S. (n.d.). Retrieved February 13, 2018, from http://wavefrontshaping.net/index.php/article-highlights/56-a-pioneer-experiment

76. Sarma, R., Yamilov, A., & Cao, H. (2017). Enhancing light transmission through a disordered waveguide with inhomogeneous scattering and loss. Applied Physics Letters, 110(2), 021103.

APPENDIX

Calculation of Transverse Parameters:

```
"In this code calculation of transverse parameters of a fiber with
  25 μm core radius and wavelength λ = 1.555 μm is explained. Eq.2.30
  is solved by numerical method. To solve the Eq.2.30 by numerical
  method, new function findAllRoots is defined. By this function, the
  intersection points in the Figure 2.3. is found"

Clear[findAllRoots]
SyntaxInformation[findAllRoots] =
  {"LocalVariables" → {"Plot", {2, 2}},
   "ArgumentsPattern" → {_, _, OptionsPattern[]}};
SetAttributes[findAllRoots, HoldAll];

Options[findAllRoots] = Join[{"ShowPlot" → False, PlotRange → All},
   FilterRules[Options[Plot], Except[PlotRange]]];

findAllRoots[fn_, {l_, lmin_, lmax_}, opts : OptionsPattern[]] :=
 Module[{pl, p, x, localFunction, brackets},
  localFunction = ReleaseHold[Hold[fn] /. HoldPattern[l] :→ x];
  If[lmin ≠ lmax,
   pl = Plot[localFunction, {x, lmin, lmax},
     Evaluate@FilterRules[Join[{opts}, Options[findAllRoots]], Options[Plot]]];
   p = Cases[pl, Line[{x__}] :→ x, Infinity];
   If[OptionValue["ShowPlot"],
    Print[Show[pl, PlotLabel → "Finding roots for this function",
      ImageSize → 200, BaseStyle → {FontSize → 8}]]], p = {}];
  brackets =
   Map[First,
    Select[(*This Split trick pretends that two points on the curve
       are "equal" if the function values have _opposite _ sign.Pairs
       of such sign-changes form the brackets for the subsequent FindRoot*)
     Split[p, Sign[Last[#2]] == -Sign[Last[#1]] &], Length[#1] == 2 &], {2}];
  x /. Apply[FindRoot[localFunction == 0, {x, ##1}] &, brackets, {1}] /. x → {}]
```

```
"V-Number of fiber as an input"

V = 2 * Pi * 0.22 * 50000 / 1555;

"To find aa transverse parameters, a loop is created. The parameter
  i represents the azimuthal component of the fiber modes.
  Transverse parameters are exported in an excel file"

Do[
 Export[
  "C:\\Users\\Halil İbrahim\\Desktop\\TEZ\\Calculations and Simulations\\1555-nm
     -Fiber-Profiles\\170201__25-um-Fiber-Profile\\Fiber-Parameters\\l=" <>
   ToString[i] <> ".xls",
  Delete[
   findAllRoots[
    x * BesselJ[i + 1, x] * BesselK[i, Sqrt[V^2 - x^2]] /
       (BesselJ[i, x] * BesselK[i + 1, Sqrt[V^2 - x^2]]) - Sqrt[V^2 - x^2], {x, 0, V}],
   Partition[
    Table[2 * i,
     {i,
      Floor[
       Length[findAllRoots[
          x * BesselJ[i + 1, x] * BesselK[i, Sqrt[V^2 - x^2]] /
             (BesselJ[i, x] * BesselK[i + 1, Sqrt[V^2 - x^2]]) - Sqrt[V^2 - x^2], {x, 0, V}]] /
        2]}], 1]]], {i, 0, 39}]
```

Calculation of Output of the Fiber

```
"In this code, the output of a multimode optical fiber is calculated.
  To calculate the output of the fiber, we use the previous transverse
  parameter calculations. Firstly, the transvers parameters are
  imported and flattened from excel files. Then, by using Eq.4.1.a
  and Eq.4.1.b., the output of the fiber is calculated. In our
  calculations, mode coupling is neglected."
```

Importing of Transverse Parameters

```
LP0n =
  Import[
   "C:\\Users\\labuser.y1-00\\Desktop\\1555-nm-Fiber-Profiles\\170201__25-um-
     Fiber-Profile\\Fiber-Parameters\\l=0.xls"];
LP0na = Flatten[LP0n, 3];
LP1n =
 Import[
  "C:\\Users\\labuser.y1-00\\Desktop\\1555-nm-Fiber-Profiles\\170201__25-um-
    Fiber-Profile\\Fiber-Parameters\\l=1.xls"];
LP1na = Flatten[LP1n, 3];
LP2n =
 Import[
  "C:\\Users\\labuser.y1-00\\Desktop\\1555-nm-Fiber-Profiles\\170201__25-um-
    Fiber-Profile\\Fiber-Parameters\\l=2.xls"];
LP2na = Flatten[LP2n, 3];

...
LP12na = Flatten[LP12n, 3];
LP13n =
 Import[
  "C:\\Users\\labuser.y1-00\\Desktop\\1555-nm-Fiber-Profiles\\170201__25-um-
    Fiber-Profile\\Fiber-Parameters\\l=13.xls"];
LP13na = Flatten[LP13n, 3];
LP14n =
  Import[
   "C:\\Users\\labuser.y1-00\\Desktop\\1555-nm-Fiber-Profiles\\170201__25-um-
     Fiber-Profile\\Fiber-Parameters\\l=14.xls"];
LP14na = Flatten[LP14n, 3];
LP15n =
 Import[
  "C:\\Users\\labuser.y1-00\\Desktop\\1555-nm-Fiber-Profiles\\170201__25-um-
    Fiber-Profile\\Fiber-Parameters\\l=15.xls"];
LP15na = Flatten[LP15n, 3];
```

```
V = 2 * Pi * 0.22 * 25000 / 1555; "The V-Number as an input"
a = {Length[LP0na], Length[LP1na], Length[LP2na], Length[LP3na],
  Length[LP4na], Length[LP5na], Length[LP6na], Length[LP7na], Length[LP8na],
  Length[LP9na], Length[LP10na], Length[LP11na], Length[LP12na],
  Length[LP13na], Length[LP14na], Length[LP15na]}; b = Flatten[a, 1];
"Random Phases are added"
t =
 Import[
  "C:\\Users\\labuser.y1-00\\Desktop\\Random-Phases\\25-um-Random-Phases.xls"];
s = Flatten[t, 3];
```

Calculation of Output of the Fiber in the Core

```
m =
  Abs[
    Sum[(BesselJ[0, LP0na[[n]] * (x^2 + y^2)^0.5 / 25] * Cos[0 * ArcTan[x, y]] *
        Exp[-I * (√((1.476 * 2 * Pi / 1.5555)^2 - (LP0na[[n]] / 25)^2) * 10^4 + s[[n]])]), {n, 1, Length[LP0na]}] +
      Sum[(BesselJ[1, LP1na[[n]] * (x^2 + y^2)^0.5 / 25] * Cos[1 * ArcTan[x, y]] *
        Exp[-I * (√((1.476 * 2 * Pi / 1.5555)^2 - (LP1na[[n]] / 25)^2) * 10^4 +
            s[[n + Length[LP0na]]])]), {n, 1, Length[LP1na]}] + ... +


     Sum[(BesselJ[14, LP14na[[n]] * (x^2 + y^2)^0.5 / 25] * Cos[14 * ArcTan[x, y]] *
        Exp[-I * (√((1.476 * 2 * Pi / 1.5555)^2 - (LP14na[[n]] / 25)^2) * 10^4 +
            s[[n + Sum[b[[n]], {n, 1, 14}]]])]), {n, 1, Length[LP14na]}] +
     Sum[(BesselJ[(n + 14), LP15na[[n]] * (x^2 + y^2)^0.5 / 25] *
       Cos[(n + 14) * ArcTan[x, y]] *
       Exp[-I * (√((1.476 * 2 * Pi / 1.5555)^2 - (LP15na[[n]] / 25)^2) * 10^4 +
            s[[n + Sum[b[[n]], {n, 1, 15}]]])]), {n, 1, Length[LP15na]}]]^2;
```

Calculation of Output of the Fiber in the Cladding

$$k = \text{Abs}\Bigg[$$

$$\sum_{n=1}^{\text{Length}[\text{LP0na}]} \left(\frac{\text{BesselJ}[0, \text{LP0na}[[n]]]}{\text{BesselK}\left[0, \sqrt{V^2 - \text{LP0na}[[n]]^2}\right]} \right.$$

$$\text{BesselK}\left[0, \sqrt{V^2 - \text{LP0na}[[n]]^2} * (x^2 + y^2)^{0.5} / 25\right] * \text{Cos}[0 * \text{ArcTan}[x, y]] *$$

$$\text{Exp}\left[-I * \left(\sqrt{(1.476 * 2 * \text{Pi} / 1.5555)^2 - \left(\sqrt{V^2 - \text{LP0na}[[n]]^2} \Big/ 25\right)^2} * 10^4 + \right.\right.$$

$$\left.\left.\left. \frac{1.46}{1.476}\, s[[n]] \right)\right]\right) +$$

$$\sum_{n=1}^{\text{Length}[\text{LP1na}]} \left(\frac{\text{BesselJ}[1, \text{LP1na}[[n]]]}{\text{BesselK}\left[1, \sqrt{V^2 - \text{LP1na}[[n]]^2}\right]} \right.$$

$$\text{BesselK}\left[1, \sqrt{V^2 - \text{LP1na}[[n]]^2} * (x^2 + y^2)^{0.5} / 25\right] * \text{Cos}[1 * \text{ArcTan}[x, y]] *$$

$$\text{Exp}\left[-I * \left(\sqrt{(1.476 * 2 * \text{Pi} / 1.5555)^2 - \left(\sqrt{V^2 - \text{LP1na}[[n]]^2} \Big/ 25\right)^2} * 10^4 + \right.\right.$$

$$\left.\left.\left. \frac{1.46}{1.476}\, s[[n + \text{Length}[\text{LP0na}]]] \right)\right]\right) + \ldots +$$

$$\sum_{n=1}^{\text{Length}[\text{LP14na}]} \left(\frac{\text{BesselJ}[14, \text{LP14na}[[n]]]}{\text{BesselK}\left[14, \sqrt{V^2 - \text{LP14na}[[n]]^2}\right]} \right.$$

$$\text{BesselK}\left[14, \sqrt{V^2 - \text{LP14na}[[n]]^2} * (x^2 + y^2)^{0.5} / 25\right] * \text{Cos}[14 * \text{ArcTan}[x, y]] *$$

$$\text{Exp}\left[-I * \left(\sqrt{(1.476 * 2 * \text{Pi} / 1.5555)^2 - \left(\sqrt{V^2 - \text{LP14na}[[n]]^2} \Big/ 25\right)^2} * 10^4 + \right.\right.$$

$$\left.\left.\left. \frac{1.46}{1.476}\, s\left[\left[n + \sum_{n=1}^{14} b[[n]]\right]\right] \right)\right]\right) +$$

```
Sum[
  (BesselJ[(n + 14), LP15na[[n]]] /
    BesselK[(n + 14), Sqrt[V^2 - LP15na[[n]]^2]]) *
   BesselK[(n + 14), Sqrt[V^2 - LP15na[[n]]^2] * (x^2 + y^2)^0.5 / 25] *
   Cos[(n + 14) * ArcTan[x, y]] *
   Exp[-I * (Sqrt[(1.476 * 2 * Pi / 1.5555)^2 - (Sqrt[V^2 - LP15na[[n]]^2] / 25)^2] * 10^4 +
        1.46/1.476 s[[n + Sum[b[[n]], {n, 1, 15}]]])],
  {n, 1, Length[LP15na]}]^2;

"Exporting output of the fiber as a matrix"

n = Table[If[(x^2 + y^2) < 625, m, k], {x, -30, 30, 0.241}, {y, -30, 30, 0.241}];
Export[
 "C:\\Users\\labuser.y1-00\\Desktop\\1555-nm-Fiber-Profiles\\170201__25-um-Fiber-
   Profile\\25-um-fiber-profile-@-z=10cmWithRandomPhase\\25-um-fiber-profile-@-z=
   10cmWithRandomPhase.xls", n]
```